Spatial Transcriptomic Analysis Reveals HDAC Inhibition Modulates Microglial Dynamics to Protect Against Ischemic Stroke in Mice

Kevin Jayaraj[1], Ritesh Kumar[1], Sukanya Shyamasundar[1] Jai S Polepalli[1], Thiruma V Arumugam[2], S Thameem Dheen[1]

[1] Department of Anatomy, Yong Loo Lin School of Medicine, National University of Singapore, Singapore 117594

[2] Centre for Cardiovascular Biology and Disease Research, Department of Microbiology, Anatomy, Physiology and Pharmacology, School of Agriculture, Biomedicine and Environment, La Trobe University, Bundoora, Victoria, Australia

Correspondence: S Thameem Dheen E-mail: antstd@nus.edu.sg

Co-Correspondence: Jai S Polepalli E-mail: jpolepalli@nus.edu.sg

Key Words

Microglia, Stroke, HDAC inhibitor, Spatial Transcriptomics, Neuroinflammation, Neuroprotection

Abstract:

Ischemic stroke significantly contributes to global morbidity and disability through a cascade of neurological responses. Microglia, the immune modulators within the brain, exhibit dual roles in exacerbating and ameliorating ischemic injury through neuroinflammatory and neuroprotective roles, respectively. Despite emerging insights into microglia's role in neuronal support, the potential of epigenetic intervention to modulate microglial activity remains largely unexplored. We have previously shown that sodium butyrate, a histone deacetylase inhibitor (HDACi) epigenetically regulates inflammatory response of microglia after ischemic stroke and this study was aimed to characterize the transcriptomic profiles of microglia and their spatial distribution in the stroke brain followed by HDACi administration. We hypothesized that the administration of HDACi epigenetically modulates microglial activation and a region-specific microglial phenotype in the stroke brain, shifting their phenotype from neurotoxic to neuroprotective and facilitating neuronal repair and recovery in the ischemic penumbra. Utilizing a rodent model of middle cerebral artery occlusion (MCAo), spatial transcriptomics and 3D morphometric reconstruction techniques were employed to investigate microglial responses in critical penumbral regions, such as the hippocampus, thalamus, cortex and striatum following HDACi administration. We found that HDACi significantly altered the microglial transcriptomic landscape involving biological pathways of neuroinflammation, neuroprotection and phagocytosis as well as morphological phenotype, promoting a shift towards reparative, neurotrophic profiles within the ischemic penumbra. These changes were also associated with enhanced neuronal survival and reduced neuroinflammation in specific regions in the ischemic brain. By elucidating the mechanisms through which HDAC inhibition influences microglial function, our findings propose therapeutic avenues for neuroprotection and rehabilitation in ischemic stroke, and possibly other neurodegenerative conditions that involve microglia-mediated neuroinflammation.

Introduction

Ischemic stroke is one of the primary causes of long-term disability and mortality worldwide, presenting a significant public health challenge by exacerbating both health and economic burdens on society (Donkor, 2018; Feigin *et al.*, 2022). Focal ischemic stroke which is characterized by abrupt cessation of blood supply to a specific region in the brain, leads to hypoxia (a deprivation of oxygen), triggering a cascade of deleterious cellular and molecular events such as excitotoxicity, neuroinflammation, and apoptosis. During reperfusion, restoration of blood flow to the infarcted tissue further aggravates tissue injury (Traystman, 2003; Mergenthaler, Dirnagl and Kunz, 2022). Complex, multicellular pathways and interactions dictate mechanisms that mediate neuronal damage post-ischemic injury and highlight the need for novel therapeutic strategies for enhancing recovery and clinical outcomes (Zhang *et al.*, 2019; Wang, Leak and Cao, 2022).

Microglia, resident immune cells of the brain are at the forefront of the body's response to ischemic injury. They exhibit a spectrum of phenotypic changes (Dubbelaar *et al.*, 2018; Wendimu and Hooks, 2022) and transition dynamically between conventional pro-inflammatory (M1) and anti-inflammatory (M2) states depending on spatial and temporal contexts after ischemia. In the stroke brain, microglia initially clear debris and release pro-inflammatory cytokines like TNF-α and interleukins, triggering neuroinflammatory responses crucial for initiating repair but turn deleterious if it progresses without biological checkpoints controlling the response (Wang, Leak and Cao, 2022). Transitioning to an anti-inflammatory phenotype, microglia release cytokines and neurotrophins promoting tissue repair and limiting ongoing damage (Gupta *et al.*, 2018; Zhang *et al.*, 2021; Charlton *et al.*, 2023). The balance between these microglial states and their heterogenous expression profiles are crucial for the prognosis of stroke. Positive modulation of microglial activation is essential in ameliorating neurodegeneration and reperfusion mediated injury, suggesting that targeted interventions aimed at microglia could offer significant therapeutic benefits (Nagy *et al.*, 2020).

Epigenetic mechanisms, such as DNA methylation, histone modification, and RNA-associated silencing, play pivotal roles in regulating microglial function and response to ischemic stroke. Histone deacetylases (HDACs) are key enzymes involved in removing acetyl groups from histones, leading to reduced gene expression that has been explored to regulate progress of pathology and neuroinflammation in stroke and other inflammatory conditions (Adcock, 2007; Fessler *et al.*, 2013; Patnala *et al.*, 2017). In the context of ischemic stroke, such epigenetic modifications influence the phenotypic switching of microglia between pro-inflammatory and anti-inflammatory states, thus affecting the overall inflammatory milieu and recovery process (Saw *et al.*, 2020; Qiu, Xu and Zhan, 2021).

Sodium butyrate, a HDAC inhibitor (HDACi), has emerged as a promising epigenetic therapy for ischemic stroke (Sun *et al.*, 2015). By modulating the epigenetic landscape, HDACi can shift microglial activation towards neuroprotective states, reducing neuroinflammation and promoting neuroprotection. This therapeutic potential is further supported by studies demonstrating its ability to enhance the expression of neurotrophic factors and modulate key signaling pathways involved in cell survival, neurogenesis, and synaptic plasticity (Patnala *et al.*, 2017; Ziemka-Nalecz *et al.*, 2017; Saw *et al.*, 2020; Li *et al.*, 2024; Xu *et al.*, 2024).

Our research leverages advanced methodologies, including high-resolution imaging, 3D microglial reconstruction, and spatial transcriptomics, to delve deeper into the effects of HDACi on microglial dynamics and their transcriptional profile in the stroke brain. By exploring biological networks relevant to microglia-neuron interaction and the impact of epigenetic modulation on microglial function, we aim to uncover novel therapeutic targets that could significantly enhance the functional outcomes in ischemic stroke therapy (Qiu, Xu and Zhan, 2021; Zhang *et al.*, 2022)

Given the intricate interplay between microglia, neurons, and other glial cells in the ischemic brain, understanding the precise molecular pathways including those affected by epigenetic modifications induced by microglial activity, is critical for developing targeted therapies for stroke. The application of HDAC inhibitors like sodium butyrate offers a unique approach to

97 modulating the brain's innate immune response, steering it towards pathways that support
98 neuroprotection, repair, and regeneration. Such insights are crucial for developing targeted
99 interventions which harness the therapeutic potential of microglial modulation in the context of
100 ischemic stroke.

101 The present study demonstrates that HDACi treatment not only reduces infarct volume in
102 stroke brain but also influences microglial phenotypes towards reparative states, facilitating
103 neuronal survival and mitigating neuroinflammation. Through analysis incorporating cutting-
104 edge spatial transcriptomic techniques, we obtain nuanced understanding of microglial roles
105 in stroke pathophysiology and recovery, paving the way for targeted therapies that can
106 capitalize on the therapeutic promise of microglial modulation.

107

108 **Methods**

109 **Ethics Statement**

110 Adult male C57Bl/6J mice, 12-15 weeks old were acquired (InVivos Pte Ltd, Singapore) and
111 housed under controlled temperature, humidity, light and dark cycles at the NUS Comparative
112 Medicine (CM) Vivarium. Mice were provided access to standard food pellets and water ad
113 libitum. Animal work was performed in accordance with the Institutional Animal Care and Use
114 Committee (IACUC) through protocol NUS/IACUC/R19-0596 approved for the experiments
115 performed with animal(s) and tissues in this study.

116

117 **Surgical Ischemic Stroke Modelling and HDACi treatment in Mice**

118 MCAo modelling was performed as previously described (Patnala *et al.*, 2017) using adult
119 male C57BL/6J mice (12-15 weeks old, 26-29g). The mice were anesthetized with isofluorane
120 in an induction chamber. Ophthalmic lubricant (Duratears 3.5g, Alcon, USA) was applied to
121 prevent corneal drying, and body temperature was monitored and maintained at 37.0 ± 0.5°C
122 with a heating pad. The neck of the mice was shaved, disinfected with 70% ethanol and

123 povidone-iodine solution, and a midline incision was made to expose the common carotid
124 artery (CCA), internal carotid artery (ICA), and external carotid artery (ECA). The CCA and
125 ICA were clamped, and the ECA was cauterized and retracted. A Doccol 6-0 monofilament
126 nylon suture (catalog no.: 602123PK10, Doccol Corporation, USA), (diameter of 0.21-0.23
127 mm), was introduced through the ECA and advanced into the ICA to occlude the MCA.
128 Occlusion was maintained for 60 minutes, after which the suture was withdrawn to allow
129 reperfusion. The ECA incision was cauterized, and the microvascular clips were removed to
130 restore blood flow through the CCA and ICA. The surgical site was sutured, and the animals
131 were allowed to recover from anaesthesia under observation. In sham group mice, surgical
132 reflection of muscles to reveal CCA bifurcation was performed without disturbing the
133 vasculature to affect cerebral blood flow. Sodium butyrate (HDACi) was administered
134 intraperitoneally (I.P.) to the mice (Cat. no. B5887-1G, Sigma-Aldrich) at a dose of 300 mg/kg
135 bodyweight. Two doses of NaBu were administered, 1-hour prior ischemia and 6-hours post
136 reperfusionas described previously (Patnala *et al.*, 2017). Mice were housed a temperature-
137 controlled environment with a 12-hour light/dark cycle and provided food and water ad libitum.
138 Motor deficit after surgical modelling was evaluated through preliminary neurological deficit
139 scoring (pNDS). Severity of motor affect through was graded on a scale of 0 to 4 (normal score
140 0, maximal deficit score 4) (n=4) (Garcia *et al.*, 1995; Li *et al.*, 2000) . Animals were regularly
141 monitored for adverse effects or complications, ensuring compliance with guidelines for the
142 care and use of laboratory animals, aimed at minimizing suffering and the number of animals
143 used. 24 hours post-stroke induction, mice were euthanized with an intraperitoneal overdose
144 of sodium pentobarbital (150 mg/kg) and absence of pedal and corneal reflexes was confirmed
145 prior to harvest of brain tissue. For histological and immunofluorescence analyses, mice were
146 perfused with ice-cold 4% paraformaldehyde (PFA) and post-fixed at 4°C for 24 hours prior to
147 histological processing. For spatial transcriptomic analyses, brain tissue was processed as
148 per 10x Genomics Visium fresh frozen tissue preparation guide CG000240 - Rev E.

149

150 **TTC Staining of mouse brain tissue and evaluation of tissue damage**

151 For 2,3,5-Triphenyltetrazolium chloride (TTC) staining, fresh brain tissue was sectioned into 2
152 mm coronal slices using a brain matrix. The brain slices were submerged in cold PBS to
153 maintain tissue viability. Freshly prepared 2% solution of TTC (Cat. no. T8877, Sigma-Aldrich)
154 was added to brain sections in a 24-well plate and incubated at 37°C for 30 minutes in a dark,
155 humidified incubator. Viable tissue stained red, while infarcted areas remained pale or white.
156 Post-incubation, sections were rinsed with PBS and transferred to a clear, flat transparent
157 sheet for digital imaging on a flatbed scanner (CanoScan LiDe 400, Canon). Image processing
158 and analysis of TTC-stained brain sections was performed by thresholding scanned images
159 to greyscale and extrapolating pixel values (Goldlust *et al.*, 1996).Scanned images were
160 loaded and processed using R packages to calculate and distinguish viable (non-infarcted)
161 and non-viable (infarcted) area in brain tissue. Viable and non-viable areas were calculated in
162 square millimeters based on pixel counts and known image resolution. Statistical analysis,
163 including t-tests and ANOVA, was performed to compare the groups (n=3).. The results were
164 then imported into Microsoft Excel for visualization.

165

166 **Histological Processing of Mouse Brain Tissue Sections**

167 Harvested brain tissues were post-fixed in 4% paraformaldehyde and dehydrated through a
168 graded series of ethanol baths and clearene. Dehydrated and cleared samples were then
169 incubated in molten paraffin wax, embedded and allowed to solidify at room temperature.
170 Solidified wax blocks were mounted onto a microtome, trimmed, and sectioned at 7μm
171 thickness. Sections were floated in a warm water bath, transferred onto microscope slides,
172 and stained with toluidine blue. Routine staining protocols were performed involving
173 deparaffinization in clearene, rehydration through descending ethanol series, staining in
174 toluidine blue followed by rinsing, dehydrating ethanol series and tissue clearing prior to
175 coverslipping slides with mounting medium (S302380-2, Dako North America Inc.). For
176 cryosectioning, PFA-fixed brain tissues were cryoprotected in 30% sucrose until fully
177 saturated, embedded in OCT compound, and rapidly frozen using dry ice or pre-cooled

178 isopentane. Frozen OCT-embedded tissue blocks were sectioned at -20°C to -25°C in a
179 cryostat (Leica Instruments GmbH, Germany), with sections cut at 30 to 50 microns, collected
180 onto chilled slides, and stored at -80°C in sealed containers with desiccants until further use.

181

182 **Immunofluorescence and Morphometric analysis**

183 Mouse brain tissues were fixed with 4% paraformaldehyde, cryoprotected in 30% sucrose and
184 embedded in OCT compound. Mouse brains were sectioned at 30 or 50 micron thickness on
185 a cryostat (Leica Instruments GmbH, Germany). The sections were permeabilized with 0.3%
186 Triton X-100 and non-specific binding sites were blocked by incubating sections in 5% normal
187 donkey serum (D9663-10ML, Sigma-Aldrich) or 1% bovine serum albumin (126615-25MLCN,
188 Merck). The sections were then incubated with primary antibodies (antibody list in table below)
189 diluted in blocking solution, overnight at 4°C. After rinsing with PBS, sections were incubated
190 with fluorescence-conjugated secondary antibodies for 1 hour at room temperature, protected
191 from light. Following this, sections were rinsed with PBS and mounted with anti-fade
192 fluorescence mounting medium (ab104135, Abcam). The stained sections were imaged using
193 a confocal microscope (FluoView 1000 and FluoView 3000, Olympus Corporation, Japan) at
194 10x, 20x, 60x and 100x objectives. Z-stacks were captured at 60x and 100x objectives with a
195 z-plane of 20-30μm with z-sections of 0.5μm. Microglia-labelled confocal, Z-stacked imaging
196 datasets were imported into IMARIS v9.5 software for 3D reconstruction and analysis of
197 microglial morphology (n=3). The 'Surpass' view was used to inspect the z-stack, and a 3D
198 volume rendering of the z-stack was created using the 'Volume' button. For morphometric
199 evaluation and analysis, the 'Surfaces' function was employed by selecting the appropriate
200 marker channel (IBA1 for microglia), setting the 'Surface Detail Level' and 'Background
201 Subtraction', and using the 'Thresholding' slider to separate cells from the background. The
202 surface creation was finalized to generate surfaces encompassing the 3D structures of the
203 labelled cells. Morphometric analysis was exported in the 'Statistics' tab, quantifying
204 parameters such as volume and surface area. Images and videos of the 3D reconstructions

205 were exported using the snapshot and animation features in IMARIS v9.5. Comparisons of
206 these parameters between groups (Sham, MCAo, and HDACi-treated) were conducted to
207 evaluate the effects of ischemic stroke and HDACi treatment on microglial morphology.

208

209 **Primary Antibodies**

Antibody	Cat no.	Dilution	Source	Host	Clonality	Application
IBA1	ab48004	1:450	Abcam PLC, Cambridge, UK	Goat	Polyclonal	IF
NeuN	ab177487	1:600	Abcam PLC, Cambridge, UK	Rabbit	Monoclonal	IF
NeuN	ab177487	1:100	Abcam PLC, Cambridge, UK	Rabbit	Monoclonal	Spatial Transcriptomics
GFAP	ab4674	1:70	Abcam PLC, Cambridge, UK	Chicken	Polyclonal	Spatial Transcriptomics
H3K27me3	9733	1:400	Cell Signaling Technology, MA, USA	Rabbit	Monoclonal	IF
H3K4me3	9751	1:400	Cell Signaling Technology, MA, USA	Rabbit	Monoclonal	IF

210
211 **Secondary Antibodies**

Antibody	Cat no.	Dilution	Source	Host	Conjugate	Application
Donkey Anti-Goat (Alexa Fluor 488)	ab150133	1:600	Abcam PLC, Cambridge, UK	Donkey	Alexa Fluor 488	IF
Donkey Anti-Rabbit (Alexa Fluor 647)	ab150063	1:600	Abcam PLC, Cambridge, UK	Donkey	Alexa Fluor 647	IF
Donkey Anti-Rabbit (Alexa Fluor 647)	ab150063	1:100	Abcam PLC, Cambridge, UK	Donkey	Alexa Fluor 647	Spatial Transcriptomics
Goat Anti-Chicken (Alexa Fluor 488)	ab150169	1:100	Abcam PLC, Cambridge, UK	Goat	Alexa Fluor 488	Spatial Transcriptomics
DAPI	D9542-10MG	1:2000	Sigma-Aldrich			Nuclear staining (spatial transcriptomics)
Hoechst 33342	R37605	2drops/ml	Invitrogen			Nuclear staining (IF)

212

213 **Spatial Transcriptomics Pipeline**

214 Fresh-frozen brain tissue samples from the three groups (n=3) were sectioned at 10 µm
215 thickness using a cryostat (Leica Instruments GmbH, Germany). Tissue optimization was
216 performed with TO slides (part no. 3000394, 10x Genomics, California, USA) and reagents as
217 per 10x Genomics user guide CG000238-RevE and involved testing permeabilization

218 durations, with six minutes selected based on tissue morphology preservation and RNA
219 quality, assessed with a Bioanalyzer (Bioanalyzer 2100 system, Agilent, Santa Clara, CA,
220 USA) (Figure 4 Supplementary Figure 1, 2). The sections were placed on Visium Spatial Gene
221 Expression slides (part no. 2000233, 10x Genomics, California, USA) ensuring precise
222 alignment and adhesion to capture areas for spatial mapping. Immunofluorescence staining
223 (as per 10x Genomics user guide CG000312-RevD) was performed using antibodies against
224 neuronal nuclei (NeuN) and glial fibrillary acidic protein (GFAP), with DAPI for nuclear staining,
225 to correlate spatial gene expression data with specific cell types and anatomical features.
226 Antibody concentrations and incubation times were optimized through preliminary titration
227 experiments as advised by 10x standard protocols, to ensure specificity and maximal signal-
228 to-noise ratios. Following immunofluorescence and tissue preparation, in situ reverse
229 transcription on the Visium Spatial slides was performed to convert localized mRNA into cDNA
230 while retaining spatial coordinates using unique molecular identifiers (UMIs) and spatial
231 barcodes. Library preparation, conducted according to Visium protocols (10x Genomics user
232 guide CG000239-RevF), included second-strand synthesis, adaptor ligation, and amplification
233 steps. Libraries were quantified and validated for quality using Novogene's (NovogeneAIT
234 Genomics, Singapore Pte Ltd) sequencing pipeline for their Illumina platform, to ensure
235 suitability for high-throughput sequencing. Sequencing was performed to a depth of 50 million
236 reads to cover the complexity of the brain transcriptome and ensure spatial resolution of gene
237 expression patterns. Sequenced spatial libraries were processed using 10X Genomics
238 SpaceRanger 2.0.1, aligning reads to the reference genome and attributing them to specific
239 spatial locations on tissue sections based on their spatial barcodes. Spatial transcriptomic
240 data was exported from Loupe Browser 6.0 into Microsoft Excel for consolidation, upload and
241 visualization; systematically organizing metrics such as Log2 Fold Change (Log2FC) values
242 for genes of interest across different tissue sections and experimental conditions. Data
243 wrappers such as venny (Oliveros, 2007), S.R. Plot (Tang *et al.*, 2023) and heatmapper.ca
244 (Babicki *et al.*, 2016) were utilized for downstream data processing and visualization. The
245 Kyoto Encyclopedia of Genes and Genomes (KEGG), the Database for Annotation,

246 Visualization, and Integrated Discovery (DAVID), and Gene Ontology (GO) profiler were
247 employed to enrich and categorize gene expression data within biological pathways, functional
248 annotations, and cellular component. Data was visualized through S.R Plot (Tang *et al.*, 2023)
249 with clusterprofiler and pathview packages in the form of enrichment bubble and ontology bar
250 plots. Venny, an interactive tool for comparing lists (Oliveros, 2007) was utilized to generate
251 comparative lists of upregulated, downregulated and rescued genes across the biological
252 groups with spatial segregation of microglial transcriptomes. Heatmaps were generated using
253 Heatmapper.ca (Babicki *et al.*, 2016) to visualize Log2FC data exported from MS Excel
254 organized into selected pathways from enrichment analyses, providing a graphical
255 representation of gene expression variations across different brain regions and treatment
256 groups.

257

258 **Statistical analyses**

259 For infarct area evaluation from TTC stained brain slices, one-way ANOVA
260 (F-statistic=32625.11, $p=2.74 \times 10^{-9}$) and independent two-sample t-tests ($<1x10^{-6}$) were
261 performed on the calculated non-viable (infarcted) areas from all three biological groups (n=3).
262 The high F-statistic value confirms that the variability between group means is much larger
263 than the variability within groups while the t-tests confirm the findings from one-way ANOVA.
264 Similarly, independent two-sample t-tests revealed significant differences (<0.05) in IMARIS
265 morphometry data focusing on microglial surface area; microglial volume exhibited significant
266 differences (<0.005) as depicted in data between Sham and MCAo, as well as between MCAo
267 and MCAo+HDACi groups. Spatial transcriptomics data processed using proprietary 10x
268 software, SpaceRanger 2.0.1 and Loupe Browser 6.0 utilizes a statistical framework based on
269 sSeq for differential expression analysis (Yu, Huber and Vitek, 2013), Moran's I for spatial
270 enrichment (Getis, 2007) and Benjamini-Hochberg correction for controlling false discovery
271 rates ($p<0.05$) natively in the transcriptomics pipeline as described in 10x Genomics
272 repositories. Online data wrappers were fed downstream data exported from Loupe Browser

273 6.0 by filtering for genes limited to the selected pathways within the microglial/neuronal
274 spatiotranscriptomes by MS Excel's VLOOKUP function and data was visualized in the form
275 of heatmaps (heatmapper.ca), enrichment bubble plots, combined Gene Ontology bar plots,
276 CNETplots for KEGG pathways-targets enriched (S.R. Plot) and Venn diagrams for
277 dysregulated gene expression across microglial spatiotranscriptomes (Venny).

278

279 **Results**

280 **HDACi treatment reduces ischemic infarct volume in the brain and enhances**
281 **preliminary locomotor function of mice post-ischemic insult.**

282 HDACi was administered intra-peritoneally to mice undergoing 1-hour ischemia and 24-hour
283 reperfusion periods in two doses. The first dose at 1-hour pre-ischemic insult to prime cells
284 and the subsequent dose post 6-hours of ischemic insult to effectively influence reperfusion
285 mediated injury. As reported earlier, MCAo was performed for 1h and reperfusion post-
286 ischemia was done for 24h prior to euthanasia (Fig.1A) (Patnala et al., 2017). Neurological
287 viability and infarct volume were assessed through toluidine blue (Nissl) staining and TTC
288 (2,3,5-Triphenyltetrazolium Chloride) (Fig.1B-C). From the staining, the extent of ischemic
289 penumbra at brain regions of interest (ROI)'s such as hippocampus, striatum, thalamus and
290 the cortex were identified to proceed with assessment of microglia-neuron interaction in
291 regions (Fig.1B). Evaluation of basic locomotor activity in mice prior to euthanasia (Fig.1D,
292 Fig.1 Supplementary Video 1) showed circling contralateral to the infarct, and reduced mobility
293 in the MCAo groups, while HDACi-treated mice did not exhibit circling and showed reduced
294 latency to move within the home cage towards enrichment shell. Substantive restoration of
295 viable neuronal soma was observed (Fig.1E-F) 24-hour after administration HDACi. Taken
296 together, the findings suggest a) successful modelling of ischemia in the mouse brain; along
297 with identification of regions of interest (ROIs) (hippocampus, thalamus, striatum and cortex)
298 in the ischemic penumbra, presenting as potential areas to target reperfusion mediated
299 neuronal damage. b) Gross evaluation of viable brain tissue and preliminary behavioural

300 performance of HDACi administration after MCAo showcases a potential restorative effect,
301 substantiating a need for further assessment of microglial contribution to ischemia-reperfusion
302 mediated neuroinflammation as well as neuroprotection.

303

304 **HDACi ameliorates neurodegeneration in brain nuclei after ischemic stroke and inhibits**
305 **microglial aggregation.**

306 The hippocampal CA3-dentate gyrus are particularly vulnerable regions of ischemic insult
307 (Einenkel and Salameh, 2024). Histological evaluation of toluidine blue stained sections of the
308 hippocampal CA3-dentate gyrus for neuronal and Nissl body aggregation, reveals a degree of
309 neuroprotection after HDACi administration (Fig.1E); preservation of Nissl bodies correlates
310 with enhanced neuronal survival (Smith et al., 2012), substantiating that HDACi confers
311 neuroprotection in vulnerable regions of the mouse brain. Confocal images (Fig.1F) showing
312 immunofluorescence expression of NeuN and IBA1 in neurons and microglia respectively, in
313 the cortex surrounding infarct periphery indicate recruitment of microglia in stroke brain while
314 there was a reduction in recruitment and alteration of microglial morphology in stroke brain
315 following HDACi treatment; implying a tempered inflammatory response that mitigates further
316 neuronal damage by fostering a more conducive environment for recovery (Lee et al., 2014).

317

318 **HDACi treatment inhibits ischemia-induced microglial phenotype in mouse brain**

319 Microglial cells that are ramified with slender processes in the sham mouse brain exhibit
320 amoeboid and reactive phenotypes in the stroke brain (Fig.2A). Upon HDACi administration,
321 microglial phenotypes shift towards a sham spectrum ramified phenotype with long and
322 slender processes (Fig.2A). Quantitative morphometric analysis by 3D-reconstruction of thick
323 tissue sections generated using IMARIS image analysis software (v9.5) reveals that microglial
324 surface area decreases while intracellular volume is increased in the stroke brain compared
325 to sham brain microglia (Fig.2B-C). However, HDACi treatment reverses the stroke microglial
326 phenotype closer to sham mice, suggesting that HDACi inhibits ischemia-induced phenotypic

327 changes in microglia (Fig.2B-C). The distinct microglial morphology observed in this study
328 represents transcriptomic profiles that may influence their role in inflammatory response and
329 neuroprotection through the course of pathophysiology after ischemic stroke.

330

331 **HDACi inhibits ischemia-induced increase in nuclear expression of histone marks**
332 **H3K27me3 and H3K4me3 in microglia**

333 Phenotypic heterogeneity of microglia in pathological conditions is regulated by epigenetics,
334 and various signaling molecules and transcription factors (Wang *et al.*, 2021). We have
335 previously shown that acetylation marks such as H3K9ac regulate the inflammatory response
336 of microglia in the stroke brain (Patnala *et al.*, 2017). In the present study, we have analyzed
337 the expression pattern of methylation marks such as H3K27me3 and H3K4me3 to understand
338 molecular mechanisms contributing to microglial phenotypic heterogeneity in the ischemic
339 brain. The nuclear expression of H3K27me3 (Fig.3A-B) and H3K4me3 (Fig.3C) appeared to
340 be remarkably elevated in microglia of the stroke brain. Upon HDACi administration, microglia
341 exhibit a more ramified phenotype with inhibition in nuclear expression of H3K27me3 and
342 H3K4me3, similar to expression patterns of sham brain microglia suggesting that microglial
343 phenotypic heterogeneity is influenced by histone mark status. Interestingly, we also found
344 neuronal cells in the hippocampal CA2-CA3 gyri (Fig.3A-B) exhibiting an inverse H3k27me3
345 expression pattern to microglia, suggesting an epigenetic feedback mechanism across
346 microglia-neuron regulatory network of histone status that warrants further study.

347

348 **Mapping of spatial transcriptome of microglia in ischemic mouse brain following HDACi**
349 **administration**

350 The spatial transcriptome profile of microglia in response to ischemic injury and HDACi
351 administration was analyzed using the 10x Genomics Visium (FF) platform. Fresh frozen brain
352 slices were immunolabelled and imaged for neurons (NeuN, red) and astroglia (GFAP, green)
353 along with DAPI (blue) on GEX Visium slides prior to library preparation for the spatial overlay

354 (Fig.4A-B). Immunoflourescence imaging and proprietary Loupe Browser v6.0 cluster overlay
355 with key ROIs, namely the hippocampus, thalamus, striatum, and cortex were marked for post
356 processing (Fig.4A). Stroke brain tissue reveals a loss of cellular heterogeneity, and distinct
357 organizational patterns present in sham brain tissue, suggesting the disruption of cellular
358 microenvironments and signaling networks upon ischemic insult (Fig.4B-C). Preliminarily, the
359 spatial transcriptomic data revealed 19 distinct cell populations based on marker gene
360 expression across the three experimental groups (Fig.4F) with a Uniform Manifold
361 Approximation and Projection (UMAP) plot demonstrating the spatial distribution of these
362 populations alongside the spatial overlay (Fig.4E, 4C). To specifically isolate the microglial
363 transcriptome, a sub-clustering approach through feature selection and thresholding in loupe
364 browser v6.5.0 was employed (Fig.4D) by leveraging a list of microglia signature genes
365 identified in recent studies (Gerrits *et al.*, 2020; Quintana *et al.*, 2022). This allowed for the
366 extraction of microglia-enriched spots from brain co-ordinates to generate distinct microglial
367 spatiotranscriptomic datasets within the four penumbra ROIs.

368

369 **HDACi alters microglial spatiotranscriptome profiles following ischemic stroke**

370 Differential expression analysis and pathway enrichment studies were carried out to
371 investigate microglial spatiotranscriptomics and their functional implications. The anatomic
372 regions of interest on the overlay of spatiotranscriptomic spots, focusing on the ischemic
373 penumbra has been demarcated using loupe browser v6.0 (Fig.5A). Four-set Venn diagrams
374 were drawn to identify region-specific, unique and commonly upregulated (Fig.5B)
375 /downregulated (Fig.5C) /rescued (Fig.5D) microglial genes across the ischemic penumbra in
376 the hippocampus, thalamus, striatum and cortex. Among the upregulated microglial genes
377 across the four regions of interest, 22% of genes (3544) was found to be commonly
378 upregulated after HDACi administration (Fig.5B). On the other hand, only 1.5% (190) of
379 microglial genes was found to be commonly downregulated across the four regions of interest
380 (Fig.5C). Additionally, the datasets of differentially expressed genes (both up/downregulated)

381 were processed to obtain microglial genes that were rescued closer to sham expression levels
382 (Fig.5D) following HDACi treatment.

383 The dysregulated microglial genes were subjected to KEGG pathway enrichment (Fig 5E) and
384 Gene Ontology (GO) (Fig.5F) analyses. Pathway analysis yields enrichment of key functional
385 pathways pivotal for neuroinflammatory response, mediating neurotrophic support, and
386 facilitating phagocytosis (Fig.5E) alongside other pathways that may be relevant to microglial
387 responses after ischemic stroke (Fig.5 Supplementary Figure 1). Regulatory signaling
388 pathways such as PI3K-Akt signaling (PIK3CA, PIK3CB, AKT1, AKT2, AKT3, PTEN), FC
389 gamma R-mediated phagocytosis (FCGR1, FCGR3, FCGR4, SYK, and PIP5K1C), MAPK
390 signaling (DUSP1, DUSP4, DUSP6, ERK1-2, cJUN, UCP4), TNF signaling (TNF, NFKB1,
391 RelA), and TGFβ signaling (TGFBR1, TGFBR2, SMAD2, SMAD3, SMAD4) pathways shed
392 light on the transformative influence of epigenetic regulators on microglial functionality in the
393 post-stroke brain environment. The genes from these pathways were found to be rescued in
394 each region of interest within the transcriptome of microglia after HDACi administration.

395

396 Thus, HDACi treatment results in a significant alteration of the microglial transcriptomic
397 landscape, with a spatial context. Pathway-enrichment (Fig.6 Supplementary File 1) and GO
398 analyses conducted for the microglial genes of hippocampus, thalamus, striatum, and cortex
399 (Fig.6 Supplementary Figure 1A-1B) revealed that HDACi alters, and rescues expression of
400 several key pathways involved in neuroprotection, inflammatory response and phagocytosis
401 after ischemic stroke (Fig.6A,6B,6C,6D). These analyses of microglial spatiotranscriptomes
402 shed light on the emphasis of these pathways describing their big-picture and region-specific
403 roles after ischemic insult. Heatmaps visualize the expression pattern of rescued transcripts
404 across the functionally relevant pathways, alongside radar plots delineating the top 50 rescued
405 targets from these pathways in each microglial spatiotranscriptome (Fig.6A,6B,6C,6D).
406 Confocal microscopy of microglia in the hippocampus (from Fig.2B), can be corroborated with

407 microglial spatiotranscriptome to draw parallels between HDACi-rescued microglial
408 transcriptome <> microglial phenotypic heterogeneity in the hippocampus (Fig 6A <> Fig.2B).

409 The spatiotranscriptomic profile of microglia across groups emphasizes the impact of HDACi
410 on microglial gene expression involved in neuroprotection. We also analyzed if HDACi
411 treatment improves neuroprotection by influencing the neuronal spatiotranscriptome in the
412 penumbra following ischemic stroke. The rescued spatiotranscriptome of penumbral neurons
413 reveal a distinct inverse expression pattern across groups in enriched pathways (Fig.7B,7C),
414 between ischemia-affected and HDACi treated mouse brains (Fig.7A) with broader
415 implications for neuroprotection, synaptic remodeling, and plasticity. This suggests a granular
416 modulatory effect of HDACi that is potentially influenced by the local microenvironment and
417 neuronal signaling to remodel microglial expression profiles.

418

419 The findings highlight the spatial and molecular heterogeneity of microglial responses to
420 ischemic injury and HDAC inhibition, emphasizing the therapeutic capabilities of epigenetic
421 modulation in ischemic stroke. The identified pathways and rescued genes provide a robust
422 framework for further exploration of microglial-neuron interactions and the development of
423 targeted therapies.

424

425 **Discussion**

426 Recent advancements in spatial transcriptomics analysis have enriched our ability to dissect
427 stroke pathophysiology by providing spatial resolution to gene expression patterns in neurons
428 and glial cells including microglia. In the current study, integration of spatial transcriptomics
429 with advanced imaging and reconstruction techniques has offered a comprehensive view of
430 microglial dynamics in the stroke brain. The MCAo model recapitulates human physiology to
431 facilitate investigating microglial responses within the ischemic brain (Chen *et al.*, 2009; Ansari
432 *et al.*, 2011), in particular the penumbra regions including the hippocampus, thalamus, striatum
433 and cortex. Microglial activation in the stroke brain appears to influence the neuronal

434 transcriptome, which is substantiated by the dysregulated transcriptional responses observed
435 in microglia and neurons of the stroke brain. This altered microglial response, which is
436 regulated by various signalling molecules and epigenetic mechanisms, can be ameliorated
437 through epigenetic intervention as observed in the present study.

438

439 **The Influence of Transcription Factors on phenotypic heterogeneity of Microglia**

440 Microglial cells are dynamic and exhibit region- and time-dependent phenotypic heterogeneity
441 in response to neuropathological conditions such as neuroinflammation and
442 neurodegeneration including ischemic stroke (Hickman *et al.*, 2018; Li *et al.*, 2020). In the
443 current study, differential expression of microglial spatiotranscriptomes associated with
444 phenotypic heterogeneity of microglia in response to ischemic stroke, particularly under the
445 modulation of HDAC inhibition was observed. This variation in microglial phenotypes
446 elucidates the interplay of transcription factors, cell-specific receptors and microglia-neuron
447 interaction; outlining the complexity behind microglial polarization such as neuroprotective or
448 neurotoxic phenotypes in the post-stroke brain (Olah *et al.*, 2011; Haroon, Miller and
449 Sanacora, 2016; Dubbelaar *et al.*, 2018).

450 In our microglial spatiotranscriptomic analysis, ischemic stroke was found to alter key
451 signalling molecular pathways involved in neurotrophic support, phagocytic activity and
452 neuroinflammation including PI3K-Akt signaling, FC gamma R-mediated phagocytosis, MAPK
453 signaling, TNF signaling, and TGFβ signaling pathways and transcription factors regulating
454 immune response such as NF-κB, STAT1/STAT3, Nrf, and PPAR family (Yang *et al.*, 2018;
455 Simpson and Oliver, 2020; Li *et al.*, 2024). Epigenetic mechanisms such as post-translational
456 histone modifications provide an additional layer of regulation to elicit cell-specific and stimuli
457 specific immune responses (Allis and Jenuwein, 2016) in the stroke brain.

458 Post-translational histone modifications determine basic transcriptional rates and the
459 magnitude of gene expression (Bannister and Kouzarides, 2011). Among the two major
460 histone modifications namely histone acetylation and histone methylation, histone acetylation

is associated with increased accessibility to transcriptional machinery leading to increased gene expression (Marmorstein and Zhou, 2014), whereas histone methylation is more complex in regulation of gene expression through repression. Different histone modification patterns of specific marks at different sites have been shown to play distinct biological roles; this prompted us to analyze the spatial transcriptome of microglia distributed in infarct penumbra of the stroke brain upon HDACi administration to understand the epigenetic control of microglia-mediated neuropathological outcomes in the stroke brain.

Modification in histone acetylation and deacetylation status, is maintained by histone acetyltransferase (HATs) and histone deacetylase (HDACs) enzymes respectively (Yang and Seto, 2007). Several studies have shown that inhibition of HDAC exerts immunomodulatory effects, specifically suppressing pro-inflammation and inducing anti-inflammatory signaling pathways (Adcock, 2007; Kulthinee *et al.*, 2022). We have previously demonstrated the HDACi-specific immunosuppression of pro-inflammatory mediators (TNFα and NOS2) and upregulation of IL10, an anti-inflammatory mediator in microglia in ischemic stroke mice model exerting neuroprotection (Patnala *et al.*, 2017).

Dynamic regulation of repressive histone methylation marks, H3K27me3 and H3K4me3 within microglia play a significant role in their response to ischemic injury and subsequent recovery processes (Cheray & Joseph, 2018; Tang et al., 2014). In the present study, markedly elevated expression of these markers were observed in microglia that are distributed in the penumbra of ischemic brain. The increased nuclear expression of these histone marks in microglia appears to reflect a response to the ischemic environment-induced transcriptional activity which may be associated with changes in migration, phagocytosis and phenotypic heterogeneity inferred through the spatial transcriptome of microglia. Remarkably, this ischemia-induced expression of H3K27me3 and H3K4me3 was found to be reverted to near sham levels in microglia upon HDACi treatment, suggesting epigenetic regulation of H3K27me3 and H3K4me3 downstream pathways that influence recovery mechanisms.

487 Further HDACi-induced suppression of H3K27me3 in microglia of ischemic brain may be
488 associated with activation of its upstream targets such as Enhancer of Zeste Homolog2
489 (EZH2) (Suppl.tab.1_averaged_MicroglialLog2FC_10X.xslx) a catalytic subunit of the
490 Polycomb Repressive Complex 2 (PRC2) (Ayata *et al.*, 2018) which has been shown to play
491 important roles in the epigenetic regulation of phagocytic clearance and pruning of synaptic
492 activity in microglia (Hong, Dissing-Olesen and Stevens, 2016; Ayata *et al.*, 2018). Further,
493 since the PRC2 complex, including EZH2 has been shown to regulate TNFα and TGFβ
494 signalling pathways (Penas and Navarro, 2018; Chen *et al.*, 2019), the increase in EZH2
495 expression post HDACi treatment in microglia may be responsible for altered expression of
496 both inflammatory and neurotrophic regulators such as TNFα and TGFβ signalling observed
497 in the current study.

498

499 **Epigenetic Regulation over Pathway-Specific Microglial transcriptomes involved in**
500 **Neuroprotection, Neuroinflammation and Phagocytosis in the Stroke Brain**

501 Impact of HDAC inhibition on microglia in stroke brain suggests spatially defined
502 transcriptomic changes as the results highlight the spatial heterogeneity of microglial
503 transcriptomes within various regions of the stroke brain. Notably this was evident as pathways
504 crucial to neuroprotection in microglia of stroke brain after HDACi treatment exhibit a
505 transcriptomic signature similar to that of the sham brain.

506 The TGF-β signaling pathway, central to immune modulation and cell differentiation, displayed
507 marked upregulation of TGFβ receptors and SMAD family genes (e.g., TGFβR1, TGFβR2,
508 SMAD 2-4) in microglia of stroke brain following HDACi treatment. In TGFβ signaling, TGFβR-
509 Smad family complexes regulate the expression of TGFβ target genes (Chandra *et al.*, 2012;
510 Taylor *et al.*, 2017; Du *et al.*, 2018) (Lin *et al.*, 2017; Zöller *et al.*, 2018; Zhu *et al.*, 2023); the
511 surge of TGF-β signaling pathway genes suggests an amplified anti-inflammatory and
512 regenerative response in microglia, potentially enhancing their interactions with neurons to
513 support tissue repair and functional recovery in stroke brain following HDACi treatment. HDACi

514 has been found to upregulate many other anti-inflammatory genes including STAT3 and
515 PPARγ indicating an induction of anti-inflammatory response of microglia in the stroke brain
516 (Patnala et al., 2017).

517

518 Further, HDACi treatment restored expression of several other TGF-β signaling pathway
519 molecules including BMP and activin receptor membrane-bound inhibitor (*BAMBI*) which
520 interferes with TGFβ or BMP pathway transduction by forming heterodimers
521 with *TGFβRI/BMPRI* (Chen *et al.*, 2023). The involvement of *BAMBI*, and various BMPs
522 highlights the diverse role of TGF-β signaling through microglia, influencing not only immune
523 responses but also neurogenesis, and synaptic plasticity (Meyers and Kessler, 2017).

524 It has been well established that microglia contribute to neuroinflammation through excessive
525 secretion of proinflammatory mediators in the stroke brain (Jayaraj *et al.*, 2019). The activation
526 of proinflammatory mediators, is regulated by mitogen-activated protein kinases (MAPK)
527 comprising of extracellular signal regulated kinase (ERK), c-Jun N-terminal kinases (JNK),
528 and p38 and nuclear factor kappa beta (NF-κβ) gene expression (Kaminska, Mota and Pizzi,
529 2016). HDAC inhibition has been shown to modulate the p38 MAPK-MK2 signaling cascade,
530 regulating microglial activation and cytokine production (Kaminska *et al.*, 2009; Kaminska,
531 Mota and Pizzi, 2016). In the present study, many of the MAPK signalling pathway genes were
532 found to be altered in microglia following ischemia and HDACi treatment. Further, in microglia
533 of stroke brain the downregulation of c-Jun upon HDACi administration appears to modulate
534 the neuroinflammatory response, promoting neuroprotection (Waetzig *et al.*, 2005). This
535 downregulation of cJun could be mediated by HDACi-induced activation of MKP-1 (DUSP1)
536 which has been shown to inactivate MAP Kinases (Eljaschewitsch *et al.*, 2006). Overall,
537 HDACi appears to shift microglial activation towards neuroprotective states, reducing
538 neuroinflammation and promoting neuroprotection through epigenetic modifications.

539

540 Further, HDACi-induced upregulation of PI3K-AKT pathway in microglia of stroke brain
541 appears to associated with neuroprotection since we have previously demonstrated that
542 microglial PI3K-AKT-BDNF pathway regulates memory and learning in neurons via long term
543 potentiation (LTP) (Saw *et al.*, 2020). In addition, HDACi treatment seems to potentiate an
544 array of neuroprotective signaling cascades such as through the upregulation of microglial
545 TrkB, a neurotrophin receptor tyrosine kinase which is a potent regulator of hippocampal LTP
546 (Minichiello, 2009).

547

548 Microglia play a crucial role in clearing debris from the stroke microenvironment through
549 phagocytosis to enhance neuroprotection (Wang, Leak and Cao, 2022). This was evident as
550 expression of FC-γ receptor-mediated phagocytosis pathway genes such as FCGR1, FCGR3,
551 FCGR4, SYK, and PIP5K1C was found to be upregulated in microglia of stroke brain in the
552 current study. Interestingly, expression of these genes was further upregulated upon HDACi
553 treatment indicating that HDACi enhances microglial response to ischemia and capacity for
554 clearing cellular debris, limiting secondary neurodegeneration and inflammation (Qiao, Liu and
555 Qie, 2023). Overall, HDACi-mediated phagocytic activity of microglia potentially ameliorates
556 exacerbated neuroinflammation in the penumbra of the stroke brain (Lai, Zhang and Wang,
557 2014; Belov Kirdajova *et al.*, 2020). Spatially, these transcripts in hippocampal microglia
558 emphasize their role in mitigating damage and promoting recovery in regions critical for
559 cognitive functions.

560

561 The microglial transcriptomic changes induced by HDACi in different penumbral regions of the
562 stroke brain showcase a shift in microglial functionality from a proinflammatory phenotype to
563 a phenotype which improves brain repair and regeneration by enhancing phagocytosis and
564 reducing neuroinflammation.

565

566 This study also shows that HDACi altered the neuronal spatiotranscriptome to promote
567 resilience and plasticity within the ischemic brain environment (Ganai, Ramadoss and
568 Mahadevan, 2016; Kitahara *et al.*, 2021). The inverse expression patterns in neurotrophic and
569 neuroprotective pathways of these neurons in sham and stroke brains suggest broader
570 implications for brain plasticity through upstream epigenetic mechanisms aimed at
571 counterbalancing ischemia-associated excitotoxicity and neuroinflammatory response to
572 promote tissue repair and reduce neuronal susceptibility to reperfusion injury (Delcuve, Khan
573 and Davie, 2012; Kitahara *et al.*, 2021).

574

575 In conclusion, our high-throughput spatio-transcriptomic analysis unravels the mechanisms by
576 which a) microglia contribute to ischemic pathology with region-specificity and b) HDACi
577 ameliorates reperfusion mediated ischemic-injury to neurons through modulation of microglial
578 transcriptome. These findings emphasize an interplay between epigenetic regulation and
579 spatial transcriptomic changes altering communication networks between microglia and
580 neurons. Understanding the molecular mechanisms by which HDACi induced phenotypic
581 changes together with altered spatial transcriptomic landscape in microglia of stroke brain
582 would provide insight into development of potential microglia-mediated therapeutic strategies
583 for brain recovery post ischemia.

584 **Funding**

585 This study was funded by the Ministry of Education, Singapore (MOE Tier2, A-0002277-00-00
586 awarded to Professor S T Dheen).

587 **Acknowledgements**

588 Components of Figure 1 have been created with BioRender.com.

589 **Author Contribution**

590 Data acquisition: **KJ, RK**. Data analysis and interpretation: **KJ, ST.** Study design and
591 conceptualization: **ST.** Writing of the original draft: **KJ, ST.** Reviewing & editing of manuscript:
592 **all authors.** Supervision: **ST.**

593 **Data Availability**:

594 High-throughput, next-generation sequencing data from spatial transcriptomic libraries in this
595 study have been submitted to the NCBI Sequence Read Archive (SRA) under BioProject
596 PRJNA1144233.

597 **Conflict of Interest Declaration**

598 The authors declare that they have conflicts of interest related to the study.

599 **Ethics Approval**

600 All experimental procedures performed *in vivo* were approved by the National University of
601 Singapore Animal Care and Use Committee.

602

603

604

605

606

607

608

609

610

611

612 **Bibliography**

613 1. Adcock, I. M. (2007) 'HDAC inhibitors as anti-inflammatory agents', *British Journal of*
614 *Pharmacology*. Wiley, 150(7), p. 829. doi: 10.1038/SJ.BJP.0707166.
615 2. Allis, C. D. and Jenuwein, T. (2016) 'The molecular hallmarks of epigenetic control',
616 *Nature Reviews Genetics*. Nature Publishing Group, 17(8), pp. 487–500. doi:
617 10.1038/nrg.2016.59.
618 3. Ansari, S. *et al.* (2011) 'Intraluminal middle cerebral artery occlusion (MCAO) model
619 for ischemic stroke with laser doppler flowmetry guidance in mice', *Journal of*
620 *Visualized Experiments*, (51), pp. 8–11. doi: 10.3791/2879.
621 4. Ayata, P. *et al.* (2018) 'Epigenetic regulation of brain region-specific microglia
622 clearance activity', *Nature Neuroscience*. Nature Publishing Group, 21(8), pp. 1049–
623 1060. doi: 10.1038/s41593-018-0192-3.
624 5. Babicki, S. *et al.* (2016) 'Heatmapper: web-enabled heat mapping for all', *Nucleic acids*
625 *research*. Nucleic Acids Res, 44(W1), pp. W147–W153. doi: 10.1093/NAR/GKW419.
626 6. Bannister, A. J. and Kouzarides, T. (2011) 'Regulation of chromatin by histone
627 modifications', *Cell Research 2011 21:3*. Nature Publishing Group, 21(3), pp. 381–
628 395. doi: 10.1038/cr.2011.22.
629 7. Belov Kirdajova, D. *et al.* (2020) 'Ischemia-Triggered Glutamate Excitotoxicity From
630 the Perspective of Glial Cells', *Frontiers in Cellular Neuroscience*. Frontiers Media SA,
631 14. doi: 10.3389/FNCEL.2020.00051.
632 8. Chandra, M. *et al.* (2012) 'Nuclear Translocation of Type I Transforming Growth Factor
633 β Receptor Confers a Novel Function in RNA Processing', *Molecular and Cellular*
634 *Biology*. Taylor & Francis, 32(12), p. 2183. doi: 10.1128/MCB.00320-12.
635 9. Charlton, T. *et al.* (2023) 'Brain-derived neurotrophic factor (BDNF) has direct anti-
636 inflammatory effects on microglia', *Frontiers in cellular neuroscience*. Front Cell
637 Neurosci, 17. doi: 10.3389/FNCEL.2023.1188672.
638 10. Chen, J. *et al.* (2009) *Animal models of acute neurological injuries*, *Animal Models of*
639 *Acute Neurological Injuries*. doi: 10.1007/978-1-60327-185-1.

640 11. Chen, J. *et al.* (2019) ‘EZH2 inhibitor DZNep modulates microglial activation and
641 protects against ischaemic brain injury after experimental stroke’, *European Journal of*
642 *Pharmacology*, 857. doi: 10.1016/j.ejphar.2019.172452.
643 12. Chen, X. *et al.* (2023) ‘BMP and activin receptor membrane bound inhibitor: BAMBI
644 has multiple roles in gene expression and diseases (Review)’, *Experimental and*
645 *Therapeutic Medicine*, 27(1). doi: 10.3892/etm.2023.12316.
646 13. Cheray, M. and Joseph, B. (2018) ‘Epigenetics control microglia plasticity’, *Frontiers in*
647 *Cellular Neuroscience*, 12(August), pp. 1–13. doi: 10.3389/fncel.2018.00243.
648 14. Delcuve, G. P., Khan, D. H. and Davie, J. R. (2012) ‘Roles of histone deacetylases in
649 epigenetic regulation: Emerging paradigms from studies with inhibitors’, *Clinical*
650 *Epigenetics*. BioMed Central, 4(1), pp. 1–13. doi: 10.1186/1868-7083-4-5/FIGURES/2.
651 15. Donkor, E. S. (2018) ‘Stroke in the 21st Century: A Snapshot of the Burden,
652 Epidemiology, and Quality of Life’, *Stroke Research and Treatment*. Hindawi Limited,
653 2018. doi: 10.1155/2018/3238165.
654 16. Du, X. *et al.* (2018) ‘SMAD4 feedback regulates the canonical TGF-β signaling
655 pathway to control granulosa cell apoptosis’, *Cell Death & Disease 2018 9:2*. Nature
656 Publishing Group, 9(2), pp. 1–12. doi: 10.1038/s41419-017-0205-2.
657 17. Dubbelaar, M. L. *et al.* (2018) ‘The Kaleidoscope of Microglial Phenotypes’, *Frontiers*
658 *in immunology*, 9(July), p. 1753. doi: 10.3389/fimmu.2018.01753.
659 18. Einenkel, A. M. and Salameh, A. (2024) ‘Selective vulnerability of hippocampal CA1
660 and CA3 pyramidal cells: What are possible pathomechanisms and should more
661 attention be paid to the CA3 region in future studies?’, *Journal of Neuroscience*
662 *Research*. John Wiley & Sons, Ltd, 102(1), p. e25276. doi: 10.1002/JNR.25276.
663 19. Eljaschewitsch, E. *et al.* (2006) ‘The endocannabinoid anandamide protects neurons
664 during CNS inflammation by induction of MKP-1 in microglial cells’, *Neuron*. Neuron,
665 49(1), pp. 67–79. doi: 10.1016/J.NEURON.2005.11.027.
666 20. Feigin, V. L. *et al.* (2022) ‘World Stroke Organization (WSO): Global Stroke Fact Sheet
667 2022’, *International Journal of Stroke*. SAGE Publications Inc., 17(1), pp. 18–29. doi:

668 10.1177/17474930211065917.
669 21. Fessler, E. *et al.* (2013) 'Potential Roles of HDAC Inhibitors in Mitigating Ischemia-
670 induced Brain Damage and Facilitating Endogenous Regeneration and Recovery',
671 *Current Pharmaceutical Design*, 19(28), pp. 5105–5120. doi:
672 10.2174/1381612811319280009.
673 22. Ganai, S. A., Ramadoss, M. and Mahadevan, V. (2016) 'Histone Deacetylase (HDAC)
674 Inhibitors - Emerging Roles in Neuronal Memory, Learning, Synaptic Plasticity and
675 Neural Regeneration', *Current Neuropharmacology*. Bentham Science Publishers,
676 14(1), p. 55. doi: 10.2174/1570159X13666151021111609.
677 23. Garcia, J. H. *et al.* (1995) 'Neurological deficit and extent of neuronal necrosis
678 attributable to middle cerebral artery occlusion in rats: Statistical validation', *Stroke*.
679 Lippincott Williams and Wilkins, 26(4), pp. 627–635. doi:
680 10.1161/01.STR.26.4.627/ASSET/D6F51A65-684F-4409-A4B6-
681 F5F58099E815/ASSETS/GRAPHIC/HS0451886005.GIF.
682 24. Gerrits, E. *et al.* (2020) 'Transcriptional profiling of microglia; current state of the art
683 and future perspectives', *GLIA*, 68(4). doi: 10.1002/glia.23767.
684 25. Getis, A. (2007) 'Reflections on spatial autocorrelation', *Regional Science and Urban*
685 *Economics*. North-Holland, 37(4), pp. 491–496. doi:
686 10.1016/J.REGSCIURBECO.2007.04.005.
687 26. Goldlust, E. J. *et al.* (1996) 'Automated measurement of infarct size with scanned
688 images of triphenyltetrazolium chloride-stained rat brains', *Stroke*. Lippincott Williams
689 and Wilkins, 27(9), pp. 1657–1662. doi:
690 10.1161/01.STR.27.9.1657/ASSET/67D2E47D-FF57-447E-A968-
691 A4899AD60E1E/ASSETS/GRAPHIC/0011F5.JPEG.
692 27. Gupta, N. *et al.* (2018) 'Recent progress in therapeutic strategies for microglia-
693 mediated neuroinflammation in neuropathologies', *Expert Opinion on Therapeutic*
694 *Targets*. Taylor & Francis, 22(9), pp. 765–781. doi: 10.1080/14728222.2018.1515917.
695 28. Haroon, E., Miller, A. H. and Sanacora, G. (2016) 'Inflammation, Glutamate, and Glia:

696 A Trio of Trouble in Mood Disorders', *Neuropsychopharmacology 2017 42:1*. Nature
697 Publishing Group, 42(1), pp. 193–215. doi: 10.1038/npp.2016.199.
698 29. Hickman, S. *et al.* (2018) 'Microglia in neurodegeneration', *Nature Neuroscience*.
699 Springer US, 21(10), pp. 1359–1369. doi: 10.1038/s41593-018-0242-x.
700 30. Hong, S., Dissing-Olesen, L. and Stevens, B. (2016) 'New insights on the role of
701 microglia in synaptic pruning in health and disease', *Current Opinion in Neurobiology*.
702 Elsevier Current Trends, 36, pp. 128–134. doi: 10.1016/J.CONB.2015.12.004.
703 31. Jayaraj, R. L. *et al.* (2019) 'Neuroinflammation: Friend and foe for ischemic stroke',
704 *Journal of Neuroinflammation*. BioMed Central Ltd., pp. 1–24. doi: 10.1186/s12974-
705 019-1516-2.
706 32. Kaminska, B. *et al.* (2009) 'MAPK Signal Transduction Underlying Brain Inflammation
707 and Gliosis as Therapeutic Target', *The Anatomical Record: Advances in Integrative*
708 *Anatomy and Evolutionary Biology*. John Wiley & Sons, Ltd, 292(12), pp. 1902–1913.
709 doi: 10.1002/AR.21047.
710 33. Kaminska, B., Mota, M. and Pizzi, M. (2016) 'Signal transduction and epigenetic
711 mechanisms in the control of microglia activation during neuroinflammation',
712 *Biochimica et Biophysica Acta (BBA) - Molecular Basis of Disease*. Elsevier, 1862(3),
713 pp. 339–351. doi: 10.1016/J.BBADIS.2015.10.026.
714 34. Kitahara, M. *et al.* (2021) 'Exercise and pharmacological inhibition of histone
715 deacetylase improves cognitive function accompanied by an increase of gene
716 expressions crucial for neuronal plasticity in the hippocampus', *Neuroscience Letters*.
717 Elsevier, 749, p. 135749. doi: 10.1016/J.NEULET.2021.135749.
718 35. Kulthinee, S. *et al.* (2022) 'Critical Functions of Histone Deacetylases (HDACs) in
719 Modulating Inflammation Associated with Cardiovascular Diseases', *Pathophysiology*.
720 Multidisciplinary Digital Publishing Institute (MDPI), 29(3), p. 471. doi:
721 10.3390/PATHOPHYSIOLOGY29030038.
722 36. Lai, T. W., Zhang, S. and Wang, Y. T. (2014) 'Excitotoxicity and stroke: Identifying
723 novel targets for neuroprotection', *Progress in Neurobiology*. Pergamon, 115(C), pp.

724 157–188. doi: 10.1016/J.PNEUROBIO.2013.11.006.
725 37. Li, L. *et al.* (2020) 'Potential microglia-based interventions for stroke', *CNS*
726 *Neuroscience & Therapeutics*. Blackwell Publishing Ltd, 26(3), pp. 288–296. doi:
727 10.1111/cns.13291.
728 38. Li, Y. *et al.* (2000) 'Intrastriatal transplantation of bone marrow nonhematopoietic cells
729 improves functional recovery after stroke in adult mice', *Journal of Cerebral Blood Flow*
730 *and Metabolism*. Lippincott Williams and Wilkins, 20(9), pp. 1311–1319. doi:
731 10.1097/00004647-200009000-00006/ASSET/IMAGES/LARGE/10.1097_00004647-
732 200009000-00006-FIG2.JPEG.
733 39. Li, Y. *et al.* (2024) 'Sodium butyrate alleviates lead-induced neuroinflammation and
734 improves cognitive and memory impairment through the ACSS2/H3K9ac/BDNF
735 pathway', *Environment International*. Pergamon, 184, p. 108479. doi:
736 10.1016/J.ENVINT.2024.108479.
737 40. Lin, E. *et al.* (2017) 'Transforming growth factor-β signaling pathway-associated genes
738 SMAD2 and TGFBR2 are implicated in metabolic syndrome in a Taiwanese
739 population', *Scientific reports*. Sci Rep, 7(1). doi: 10.1038/S41598-017-14025-4.
740 41. Marmorstein, R. and Zhou, M. M. (2014) 'Writers and Readers of Histone Acetylation:
741 Structure, Mechanism, and Inhibition', *Cold Spring Harbor Perspectives in Biology*.
742 Cold Spring Harbor Laboratory Press, 6(7). doi: 10.1101/CSHPERSPECT.A018762.
743 42. Mergenthaler, P., Dirnagl, U. and Kunz, A. (2022) 'Ischemic Stroke: Basic
744 Pathophysiology and Clinical Implication', *Neuroscience in the 21st Century: From*
745 *Basic to Clinical: Third Edition*. Springer International Publishing, pp. 3807–3827. doi:
746 10.1007/978-3-030-88832-9_97/COVER.
747 43. Meyers, E. A. and Kessler, J. A. (2017) 'TGF-β Family Signaling in Neural and
748 Neuronal Differentiation, Development, and Function', *Cold Spring Harbor*
749 *Perspectives in Biology*. Cold Spring Harbor Laboratory Press, 9(8). doi:
750 10.1101/CSHPERSPECT.A022244.
751 44. Minichiello, L. (2009) 'Long-term potentiation Synaptic plasticity TrkB signalling

752 pathways in LTP and learning', *Nature Reviews Neuroscience*, 10.

753 45. Nagy, E. E. *et al.* (2020) 'Neuroinflammation and microglia/macrophage phenotype
754 modulate the molecular background of post-stroke depression: A literature review',
755 *Experimental and Therapeutic Medicine*. Spandidos Publications, 20(3), p. 2510. doi:
756 10.3892/ETM.2020.8933.

757 46. Olah, M. *et al.* (2011) 'Microglia Phenotype Diversity', *CNS & Neurological Disorders -*
758 *Drug Targets*, 10(1), pp. 108–118. doi: 10.2174/187152711794488575.

759 47. Oliveros, J. C. (2007) *Venny. An Interactive Tool for Comparing Lists with Venn's*
760 *Diagrams. - References - Scientific Research Publishing*, *Csic*.

761 48. Patnala, R. *et al.* (2017) 'HDAC Inhibitor Sodium Butyrate-Mediated Epigenetic
762 Regulation Enhances Neuroprotective Function of Microglia During Ischemic Stroke',
763 *Molecular Neurobiology*, 54(8), pp. 6391–6411. doi: 10.1007/s12035-016-0149-z.

764 49. Penas, C. and Navarro, X. (2018) 'Epigenetic modifications associated to
765 neuroinflammation and neuropathic pain after neural trauma', *Frontiers in Cellular*
766 *Neuroscience*. Frontiers Media S.A., p. 158. doi: 10.3389/fncel.2018.00158.

767 50. Qiao, C., Liu, Z. and Qie, S. (2023) 'The Implications of Microglial Regulation in
768 Neuroplasticity-Dependent Stroke Recovery', *Biomolecules 2023, Vol. 13, Page 571*.
769 Multidisciplinary Digital Publishing Institute, 13(3), p. 571. doi:
770 10.3390/BIOM13030571.

771 51. Qiu, M., Xu, E. and Zhan, L. (2021) 'Epigenetic Regulations of Microglia/Macrophage
772 Polarization in Ischemic Stroke', *Frontiers in Molecular Neuroscience*. Frontiers Media
773 S.A., 14, p. 697416. doi: 10.3389/FNMOL.2021.697416/BIBTEX.

774 52. Quintana, J. F. *et al.* (2022) 'Single cell and spatial transcriptomic analyses reveal
775 microglia-plasma cell crosstalk in the brain during Trypanosoma brucei infection',
776 *Nature Communications*, 13(1). doi: 10.1038/s41467-022-33542-z.

777 53. Saw, G. *et al.* (2020) 'Epigenetic regulation of microglial phosphatidylinositol 3-kinase
778 pathway involved in long-term potentiation and synaptic plasticity in rats', *Glia*, 68(3),
779 pp. 656–669. doi: 10.1002/glia.23748.

780 54. Simpson, D. S. A. and Oliver, P. L. (2020) 'ROS Generation in Microglia:
781 Understanding Oxidative Stress and Inflammation in Neurodegenerative Disease',
782 *Antioxidants*. MDPI AG, 9(8), p. 743. doi: 10.3390/antiox9080743.
783 55. Sun, J. *et al.* (2015) 'Neuroprotective Effect of Sodium Butyrate against Cerebral
784 Ischemia/Reperfusion Injury in Mice', *BioMed Research International*. Hindawi
785 Publishing Corporation, 2015. doi: 10.1155/2015/395895.
786 56. Tang, D. *et al.* (2023) 'SRplot: A free online platform for data visualization and
787 graphing', *PLOS ONE*. Public Library of Science, 18(11), p. e0294236. doi:
788 10.1371/JOURNAL.PONE.0294236.
789 57. Tang, Y. *et al.* (2014) 'Jmjd3 is essential for the epigenetic modulation of microglia
790 phenotypes in the immune pathogenesis of Parkinson's disease', *Cell Death and*
791 *Differentiation*. Nature Publishing Group, 21(3), pp. 369–380. doi:
792 10.1038/cdd.2013.159.
793 58. Taylor, R. A. *et al.* (2017) 'TGF-β1 modulates microglial phenotype and promotes
794 recovery after intracerebral hemorrhage', *Journal of Clinical Investigation*, 127(1). doi:
795 10.1172/JCI88647.
796 59. Traystman, R. J. (2003) 'Animal models of focal and global cerebral ischemia', *ILAR*
797 *Journal*. Institute for Laboratory Animal Research, 44(2), pp. 85–95. doi:
798 10.1093/ILAR.44.2.85.
799 60. Waetzig, V. *et al.* (2005) 'c-Jun N-terminal kinases (JNKs) mediate pro-inflammatory
800 actions of microglia', *Glia*. Glia, 50(3), pp. 235–246. doi: 10.1002/GLIA.20173.
801 61. Wang, L. *et al.* (2021) 'Epigenetic Modulation of Microglia Function and Phenotypes in
802 Neurodegenerative Diseases', *Neural Plasticity*, 2021. doi: 10.1155/2021/9912686.
803 62. Wang, Y., Leak, R. K. and Cao, G. (2022) 'Microglia-mediated neuroinflammation and
804 neuroplasticity after stroke', *Frontiers in Cellular Neuroscience*. Frontiers Media S.A.,
805 16, p. 980722. doi: 10.3389/FNCEL.2022.980722/BIBTEX.
806 63. Wendimu, M. Y. and Hooks, S. B. (2022) 'Microglia Phenotypes in Aging and
807 Neurodegenerative Diseases', *Cells*. Multidisciplinary Digital Publishing Institute

808 (MDPI), 11(13). doi: 10.3390/CELLS11132091.

809 64. Xu, Y. *et al.* (2024) 'Sodium butyrate activates the KATP channels to regulate the
810 mechanism of Parkinson's disease microglia model inflammation', *Immunity,*
811 *Inflammation and Disease*. John Wiley & Sons, Ltd, 12(3), p. e1194. doi:
812 10.1002/IID3.1194.

813 65. Yang, S. J. *et al.* (2018) 'The NLRP3 Inflammasome: An Important Driver of
814 Neuroinflammation in Hemorrhagic Stroke', *Cellular and Molecular Neurobiology*.
815 Springer US, 38(3), pp. 595–603. doi: 10.1007/s10571-017-0526-9.

816 66. Yang, X. J. and Seto, E. (2007) 'HATs and HDACs: From structure, function and
817 regulation to novel strategies for therapy and prevention', *Oncogene*. doi:
818 10.1038/sj.onc.1210599.

819 67. Yu, D., Huber, W. and Vitek, O. (2013) 'Shrinkage estimation of dispersion in Negative
820 Binomial models for RNA-seq experiments with small sample size', *Bioinformatics*.
821 Oxford Academic, 29(10), pp. 1275–1282. doi: 10.1093/BIOINFORMATICS/BTT143.

822 68. Zhang, F. *et al.* (2022) 'Regulation of N6-methyladenosine (m6A) RNA methylation in
823 microglia-mediated inflammation and ischemic stroke', *Frontiers in Cellular*
824 *Neuroscience*. Frontiers Media S.A., 16, p. 955222. doi:
825 10.3389/FNCEL.2022.955222/BIBTEX.

826 69. Zhang, H. *et al.* (2019) 'Isosteviol Sodium Protects against Ischemic Stroke by
827 Modulating Microglia/Macrophage Polarization via Disruption of GAS5/miR-146a-5p
828 sponge', *Scientific Reports 2019 9:1*. Nature Publishing Group, 9(1), pp. 1–16. doi:
829 10.1038/s41598-019-48759-0.

830 70. Zhang, W. *et al.* (2021) 'Microglia-associated neuroinflammation is a potential
831 therapeutic target for ischemic stroke', *Neural Regeneration Research*. Wolters Kluwer
832 Medknow Publications, 16(1), p. 6. doi: 10.4103/1673-5374.286954.

833 71. Zhu, K. *et al.* (2023) 'Disrupting microglial TGF-β signaling triggers region-specific
834 pathology in the spinal cord', *bioRxiv*. Cold Spring Harbor Laboratory, p.
835 2023.04.24.538074. doi: 10.1101/2023.04.24.538074.

836 72. Ziemka-Nalecz, M. *et al.* (2017) 'Sodium Butyrate, a Histone Deacetylase Inhibitor,
837 Exhibits Neuroprotective/Neurogenic Effects in a Rat Model of Neonatal Hypoxia-
838 Ischemia', *Molecular Neurobiology*, 54(7), pp. 5300–5318. doi: 10.1007/s12035-016-
839 0049-2.
840 73. Zöller, T. *et al.* (2018) 'Silencing of TGFβ signalling in microglia results in impaired
841 homeostasis', *Nature Communications 2018 9:1*. Nature Publishing Group, 9(1), pp.
842 1–13. doi: 10.1038/s41467-018-06224-y.
843

844 **Figure Legend:**

845

846 **Figure 1: Middle cerebral artery occlusion and gross neurological status upon HDACi**
847 **treatment.**

848 (A) Graphical pipeline describing ischemic stroke modelling in the rodent brain, ischemia-
849 associated microglia and phenotypes. (B) Toluidine blue (nissl) staining of brain tissue
850 sections with MCAo and Sham showcasing infarct extent and anatomical regions of interest
851 (ROI) covered under the penumbra. (C) Epigenetically mediated protection through HDACi
852 attenuates infarct volume 24hours post ischemic insult (TTC or 2,3,5-Triphenyltetrazolium
853 Chloride assessment of brain slices exhibit substantial recovery of viable brain tissue upon
854 NaBu administration) (n=3 in each experimental group). (D) Qualitative assessment of
855 ischemic affect through preliminary neurological deficit scoring (pNDS) demonstrates
856 enhanced locomotor activity without immobility or circling and reduced locomotor latency
857 reduction (to reach enrichment shell within home cage) after HDACi treatment (n=4 in each
858 experimental group). (E) Toluidine blue stained mouse brain sections of dentate gyrus neurons
859 in the Hippocampus exhibit variance in infarct intensity and neuronal damage post-ischemic
860 stroke with HDACi administration. (F) Immunostained confocal images of NeuN (channel AF
861 674, false-colored green) and IBA1 (channel AF488, false-colored red) appear to display
862 preserved neuronal organization in the penumbral cortex and reduced microglial aggregation
863 at the infarct periphery upon HDAC inhibition. Nucleus is stained with Hoechst 33342 (blue).

864

865 **Figure 1 Supplementary Figure 1**

866 TTC (2,3,5-Triphenyltetrazolium Chloride) treated mouse brain sections across biological
867 groups showcasing extent of infarct through viable (stained, red) tissue and non-viable
868 (unstained, white) tissue. (n=3 in each experimental group).

869

870 **Figure 1 Supplementary Video 1**

871 Assessment of ischemic stroke affect through preliminary neurological deficit scoring (pNDS);
872 video capture of each biological group showcases mild-moderate immobility and circling
873 behaviour in the MCAo group while sham and HDACi-treated groups exhibit reduced to nil
874 locomotor defects such as circling and difficulty reaching enrichment shell within home cage.

875

876 **Figure 2. Microglial morphometric assessment through surface reconstruction with**
877 **IMARIS 9.5**

878 (A) High-resolution confocal images of Microglia stained with IBA1 (channel AF 488, green)
879 reveal diverse morphological phenotypes between biological groups (n=3 in each
880 experimental group). (B) Individual microglial cells were segmented and processed across
881 groups to obtain surface area and cellular volume morphometric data. 3D-reconstruction of
882 microglial surfaces spotlights microglia with ramified and long, slender processes in HDACi
883 inhibitor administered mouse brain reminiscent of sham brain microglia while MCAo brain
884 microglia are amoeboid with substantial depth across the z-stack. (C) Microglial surface area
885 and intracellular volume are inverse between stroke and epigenetically treated groups,
886 presenting a phenotypic reversal of microglia in the penumbra.

887

888 **Figure 2 Supplementary Video 1**

889 Video capture of IMARIS 9.5 reconstructions (30μm thick, z-stacked sections), showcasing
890 surface creation and segmentation of labelled microglial cells (IBA1, AF488, false-colored red)
891 that are processed to obtain morphometric data such as surface area and cellular volume to
892 evaluate phenotypic status of microglia in the stroke brain after HDACi treatment (n=3 in each
893 experimental group)

894

895 **Figure 3. HDAC inhibition and histone mark status in microglia after ischemic stroke**

896 (A-B) Hyper-intense expression of H3K27me3 (channel 647, false-colored green) in MCAo
897 brain microglia (IBA1, channel 488, false-colored red) appear to be rescued towards sham
898 expression levels in hippocampal microglia from HDACi-treated stroke brains. Potential
899 shuttling of H3K27me3 suggests upstream involvement of the PRC2 complex and EZH2,
900 components mediating H3K27me3-related gene silencing upon ischemic insult. (C) Similar to
901 H3K27me3, H3K4me3 (channel 647, false-colored green) expression levels in sham and
902 HDACi-treated stroke brain tissue showcase similar expression patterns with stroke elevating
903 expression in microglial nuclei suggesting neuron-microglia regulatory networks activated by
904 HDACi administration.

905

906 **Figure 3 Supplementary Figure 1**

907 (A,B,C) Tilescan (10x) images of complete brain sections across biological groups; (D,E,F)
908 showcasing hippocampal expression of H3K27me3 (AF647, false-colored green) in microglia
909 stained with IBA1 (AF488, false-colored red) that is upregulated upon ischemic stroke and
910 ameliorated upon HDACi-treatment.

911

912 **Figure 3 Supplementary Video 1**

913 Video capture of (30μm thick, z-stacked sections) microglia stained with IBA1 (AF488, false-
914 colored red) and H3K27me3 (AF647, false-colored green) across all three biological groups,
915 showcasing elevation of histone mark expression and presence within the nuclei of microglial
916 cells.

917

918 **Figure 4. Spatial transcriptome pipeline: regions of interest, population clusters and**
919 **microglial spatiotranscriptomic signature with the Visium Fresh Frozen platform (10x**
920 **Genomics)**

921 (A) Immunofluorescence (IF) image and spatial (spot) overlay (B) of Visium fresh frozen
922 sections and marker gene population clusters (C) (n=3 in each experimental group). (B) 10x
923 Genomics proprietary Loupe Browser 6.0's default transcriptome overlay represented as k-
924 clusters and population identities; (C) the distinct population clusters appear to lose
925 organization upon ischemic insult. (D) Microglial spots enriched through microglia signature
926 genes adapted from (Gerrits *et al.*, 2020; Quintana *et al.*, 2022) performed through Loupe
927 browser 6.0's feature selection and thresholding to output microglia-specific spatial
928 transcriptomes segmented based on regions on interest in the tissue section. (E) Heatmap of
929 total spatial library with cell signature markers for processed brain samples exhibiting 19
930 population identities. (F) Uniform Manifold Approximation and Projection (UMAP) dimension
931 reduction of all cell populations in the dataset.

932

933 **Figure 4 Supplementary Figure 1**

934 (A,B) Tissue optimization timepoint experiments for brain samples with 10x Genomics Visium-
935 TO slides for evaluation of optimum cDNA permeabilization time points (10x UG CG000238-
936 RevE) prior to proceeding with gene expression and library preparation of Visium fresh-frozen
937 spatial libraries. 6 minutes of permeabilization was selected based on optimization time points
938 evaluated. (C) Antibody titre evaluation for IF-staining of spatial tissue sections (10x UG
939 CG000312-RevD) identified concentration of antibodies (table in methodology).

940

941 **Figure 4 Supplementary Figure 2**

942 Permeabilized Visium fresh-frozen slides and quality control (QC) of RNA integrity checks and
943 pre-cDNA amplification/ cleanup for visium libraries prior to preparation and sequencing.

944

945 **Figure 5. Spatial segmentation of microglial transcriptomes was performed and**
946 **expression signatures across the ischemic penumbra to obtain functionally relevant**
947 **enriched pathways (KEGG).**

948 (A) Grouping and segmentation of Penumbra regions of interest in *LoupeBrowser* for spatial
949 demarcation of microglia after ischemic stroke. (B, C, D) Four-set Venn diagrams of unique
950 and overlapping HDACi-Upregulated (B), Downregulated (C) and Rescued (D) Genes,
951 elucidate the homogenous and heterogenous marks in microglia across brain regions.
952 Pathway (Kegg) Enrichment (E) and Gene Ontology (F) analysis of genes dysregulated
953 homogenously across the four microglial spatiotranscriptomes are processed and showcase
954 potential microglial pathways of interest to analyze and target after ischemic stroke. (n=3 for
955 each experimental group)

956

957 **Figure 5 Supplementary Figure 1**

958 Alternative enriched (KEGG) pathways from commonly dysregulated genes of microglial
959 spatiotranscriptomes across all 4 ROIs (hippocampus, thalamus, striatum, cortex). These
960 pathways present additional targets and mechanisms that may be dysregulated throughout
961 penumbral microglia after ischemic stroke and HDACi-administration.

962

963 **Figure 6. Microglial spatiotranscriptome expression of enriched, key biological**
964 **pathways after HDACi administration in ischemic stroke.**

965 Heatmaps of microglial spatiotranscriptomes of each ROI, hippocampal (A), thalamic (I),
966 striatal (J), cortical (K) microglia exhibit differential profiles of selected biological pathways that

967 were enriched and involved in ischemic injury across the three biological groups (n=3 for each
968 experimental group). Rescued genes within identified pathways crucial for neuroprotective,
969 neuroinflammatory and phagocytosis mediation responses are represented, and top 50
970 targets represented, in the radar plot for each penumbra ROI.

971

972 **Figure 6 Supplementary Figure 1A**

973 Pathways enriched in HDACi-rescued, region-specific microglial spatiotranscriptomes
974 (hippocampus-A, thalamus-B, striatum-C, cortex-D). Evaluation of pathways rescued by
975 HDACi after ischemic injury, highlights pathways crucial for neuroprotective,
976 neuroinflammatory and phagocytosis mediation responses.

977

978 **Figure 6 Supplementary Figure 1B**

979 Gene Ontology analyses of region-specific, microglial spatiotranscriptomes (hippocampus-A,
980 thalamus-B, striatum-C, cortex-D) exhibit differential GO terms in respective compartments
981 (BP, CC and MF) involved in HDACi-mediated rescue after ischemic injury in microglia.

982

983 **Figure 6 Supplementary Figure 2**

984 Heatmaps representing all dysregulated genes within selected biological pathways (HDACi vs
985 MCAo Log2fc difference>1.0, Euclidean distance metric with hierarchical clustering through
986 complete linkage) in each penumbra microglial spatiotranscriptomes (hippocampus-A,
987 thalamus-B, striatum-C, cortex-D). Microglial heterogeneity in expression patterns of these
988 pathways further highlights the specificity of microglial responses to ischemic stroke and
989 HDACi therapy based on spatial contexts within the mouse brain.

990

991 **Figure 6 Supplementary Figure 3**

992 Circular Network Plot (cnetplot) of HDACi-rescued pathways and targets in each microglial
993 spatiotranscriptome (hippocampus-A, thalamus-B, striatum-C, cortex-D) post-ischemic stroke.
994 Genes (nodes) are positioned around the plot, sized by log2 fold change (log2FC) and colored
995 from red (upregulated) to blue (downregulated). Pathway nodes are centrally located, sized
996 by the number of associated genes, and color-coded by functional categories. Key pathways
997 identified in the study including "MAPK signaling," "PI3K-Akt signaling," and "Fc gamma R-
998 mediated phagocytosis." are depicted with lines indicating gene-pathway associations,
999 illustrating the molecular interactions affected by HDACi treatment.

1000

1001 **Figure 7. Penumbra Neuronal Spatiotranscriptome**

1002 (A-B) Spatiotranscriptome of penumbral neurons showcases enriched neuronal pathways
1003 relevant for survival through HDACi-mediated rescue after ischemic stroke. (C) Distinct,
1004 inverse expression profiles after HDACi treatment can be observed, indicating context-
1005 dependent microglia-neuron interaction upon ischemic stroke and epigenetic regulation
1006 through HDACi. (n=3 for each experimental group)

1007

1008 **Figure 2. Supplementary File 1**

1009 Morphometry data table consisting of IMARIS *Surfaces* feature metrics (Volume, Surface Area
1010 of microglial cells)

1011

1012

1013 **Figure 6. Supplementary File 1**

1014 Enriched Kyoto Encyclopedia of Genes and Genomes (KEGG) pathways of interest from
1015 individual microglial spatiotranscriptomes.

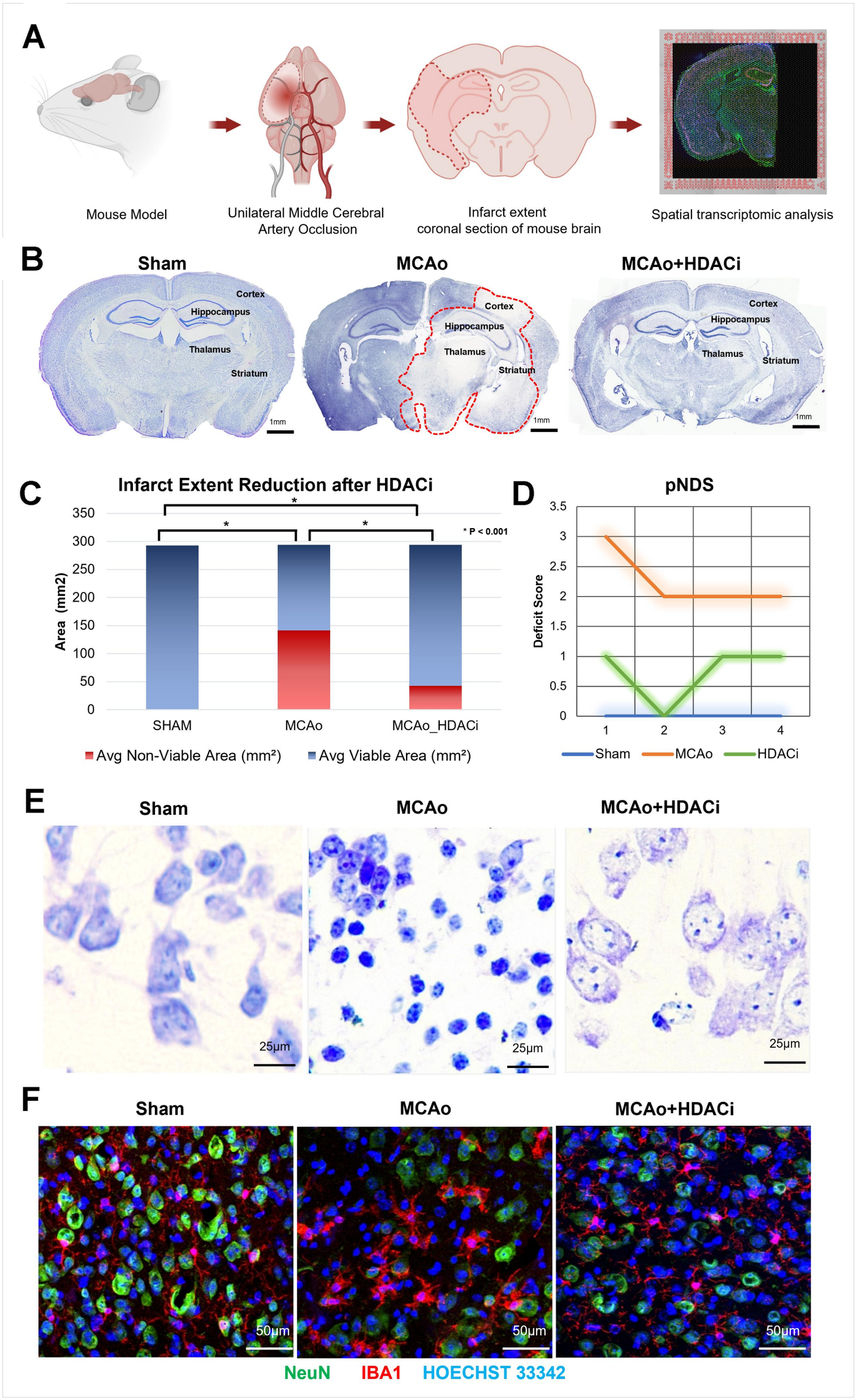
A
Mouse Model
Unilateral Middle Cerebral Artery Occlusion
Infarct extent coronal section of mouse brain
Spatial transcriptomic analysis
B
Sham
MCAo
MCAo+HDACi
Cortex
Hippocampus
Thalamus
Striatum
1mm
C
Infarct Extent Reduction after HDACi
Area (mm2)
350
300
250
200
150
100
50
0
*
* P < 0.001
SHAM
MCAo
MCAo_HDACi
Avg Non-Viable Area (mm²)
Avg Viable Area (mm²)
D
pNDS
Deficit Score
3.5
3
2.5
2
1.5
1
0.5
0
1
2
3
4
Sham
MCAo
HDACi
E
Sham
MCAo
MCAo+HDACi
25μm
F
Sham
MCAo
MCAo+HDACi
50μm
NeuN
IBA1
HOECHST 33342

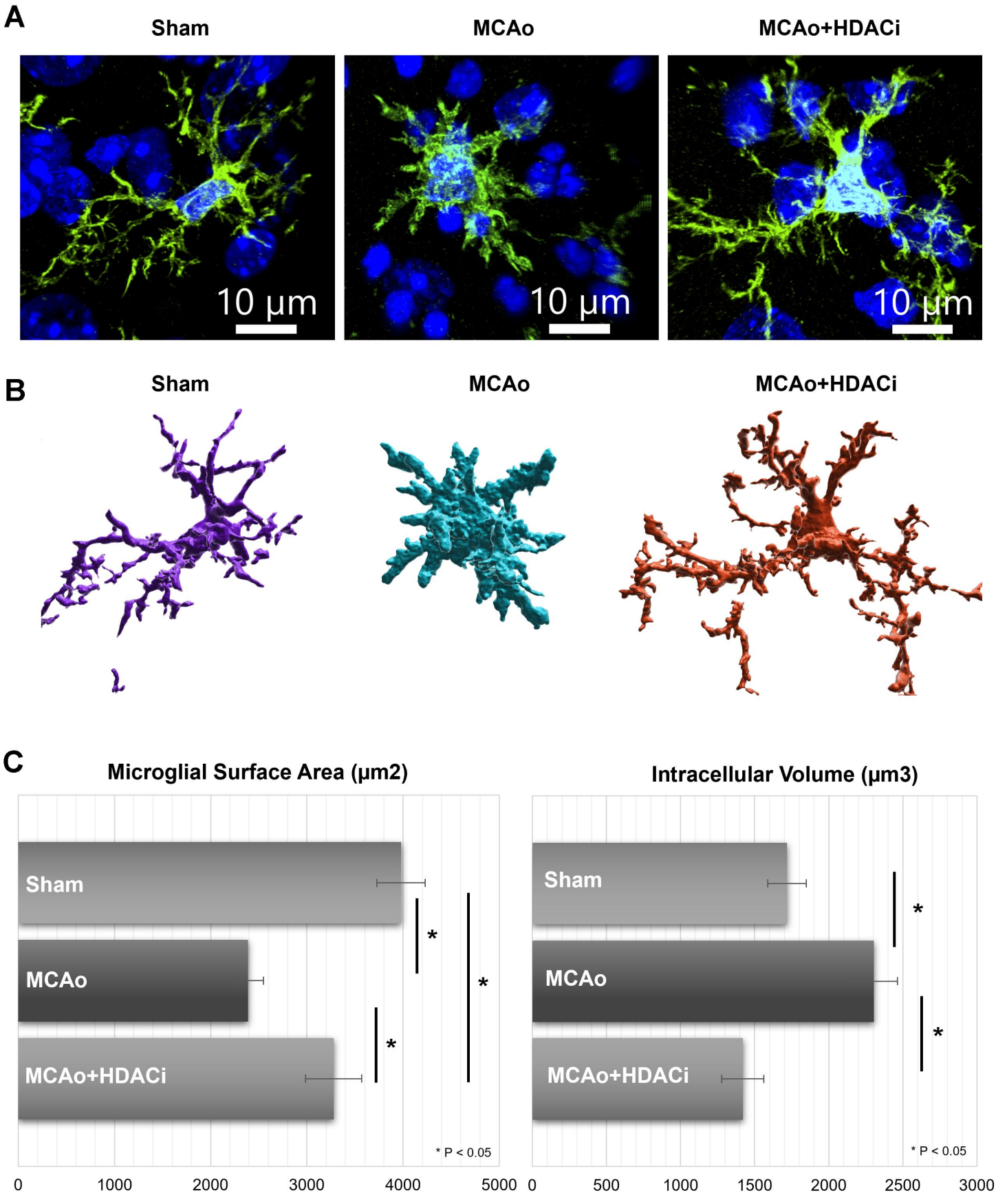
A
Sham
MCAo
MCAo+HDACi
10 µm
10 µm
10 µm
B
Sham
MCAo
MCAo+HDACi
C
Microglial Surface Area (µm2)
Sham
MCAo
MCAo+HDACi
*
*
*
* P < 0.05
0
1000
2000
3000
4000
5000
Intracellular Volume (µm3)
Sham
MCAo
MCAo+HDACi
*
*
* P < 0.05
0
500
1000
1500
2000
2500
3000

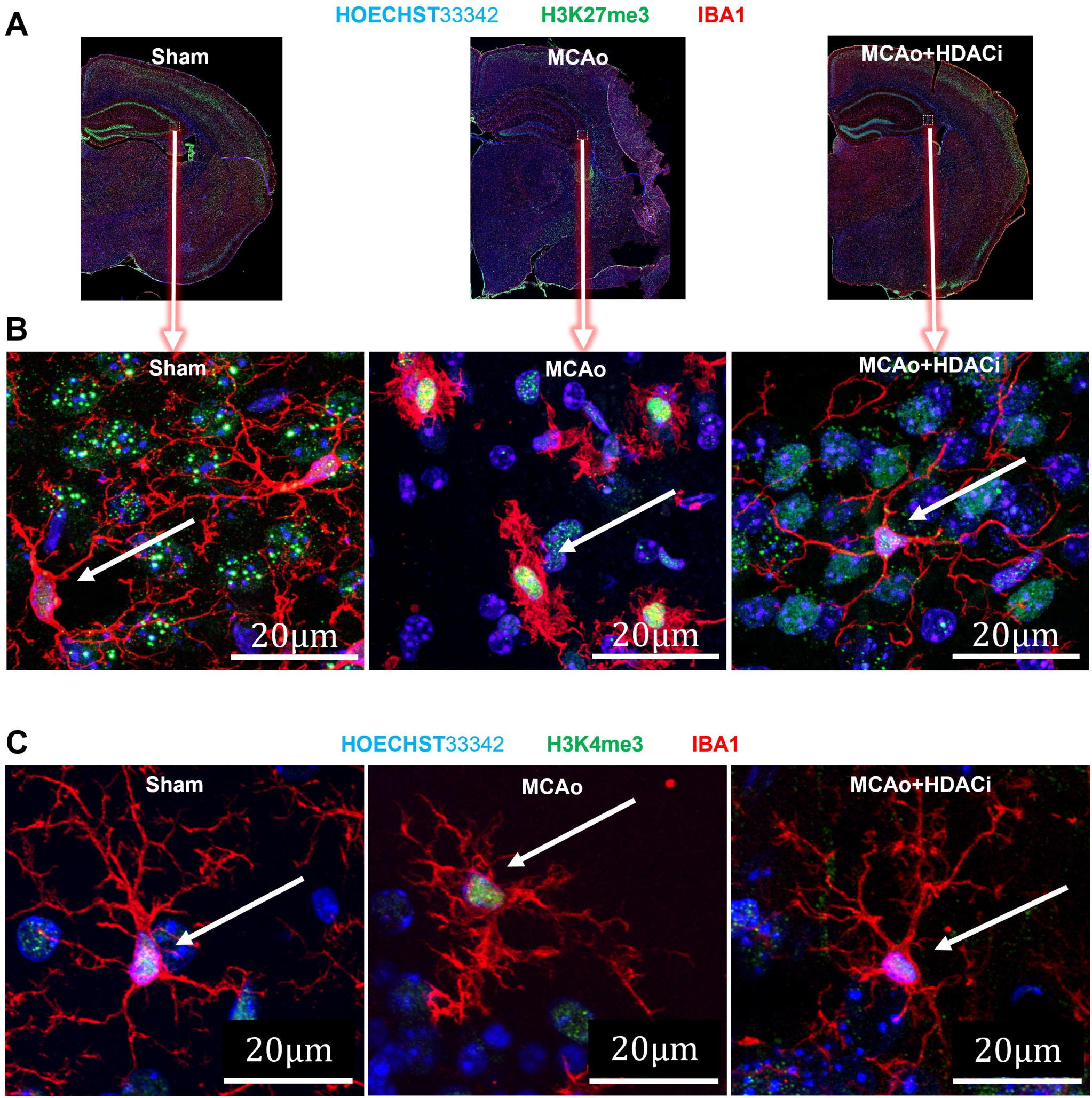
A
HOECHST33342
H3K27me3
IBA1
Sham
MCAo
MCAo+HDACi
B
Sham
MCAo
MCAo+HDACi
20μm
20μm
20μm
C
HOECHST33342
H3K4me3
IBA1
Sham
MCAo
MCAo+HDACi
20μm
20μm
20μm

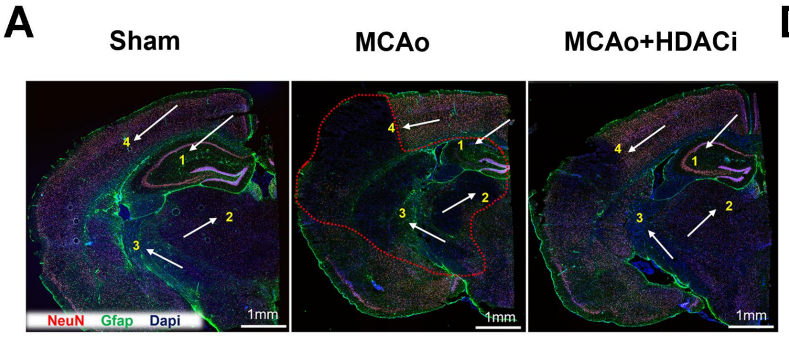

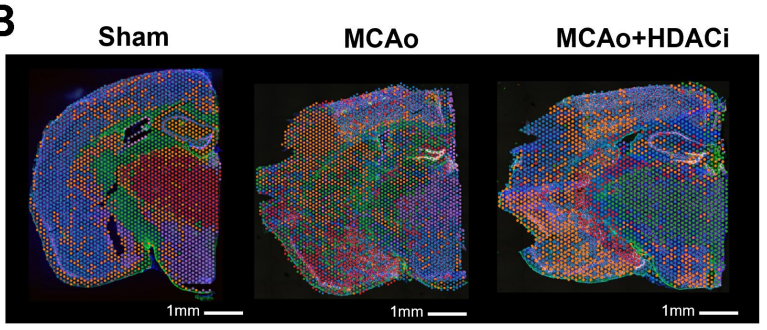

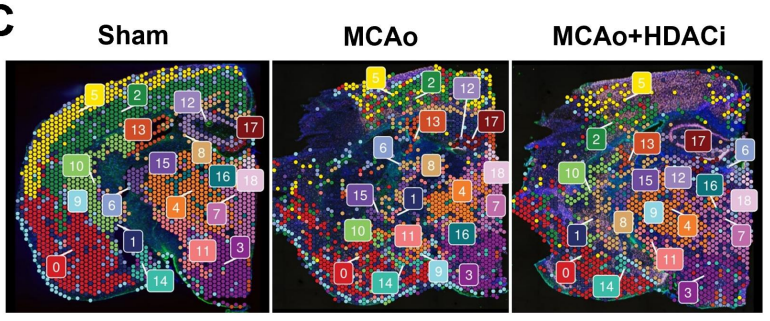

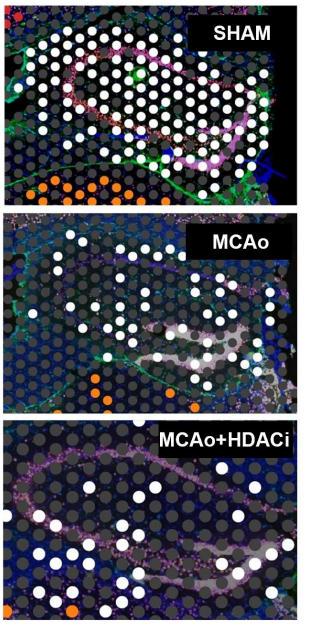

Microglial signature genes (Quintana et al., 2022) (Gerrits et al., 2020)	
P2ry12	Tmem119
Sall1	Trem2
Trem119	P2ry12
Hexb	Mertk
Cx3cr1	Pros1
Fcrls	Aif1
Gpr43	Siglech
Cx3cr1	

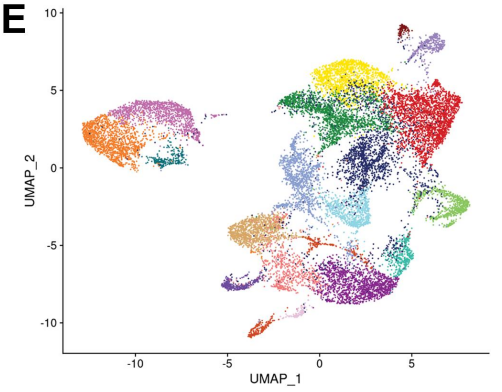

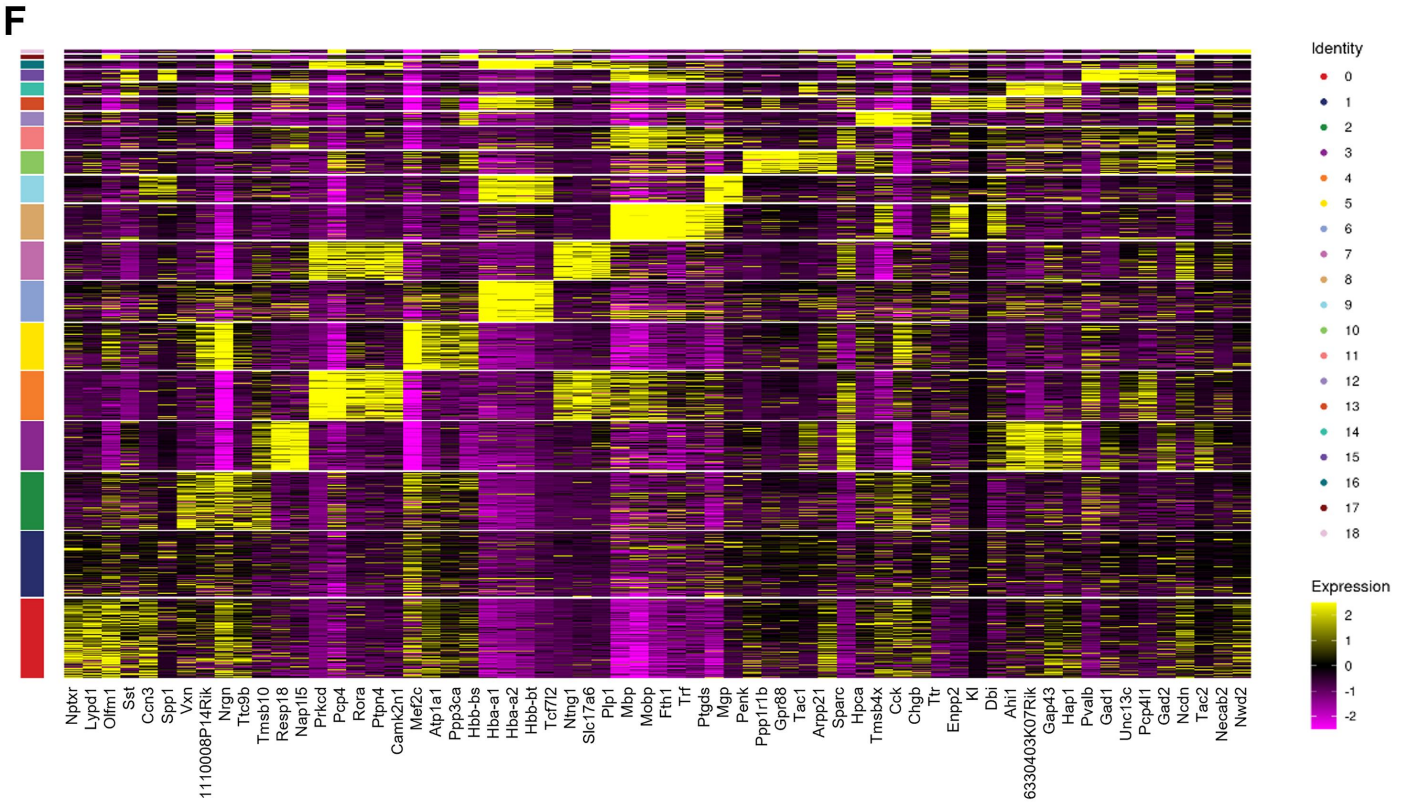

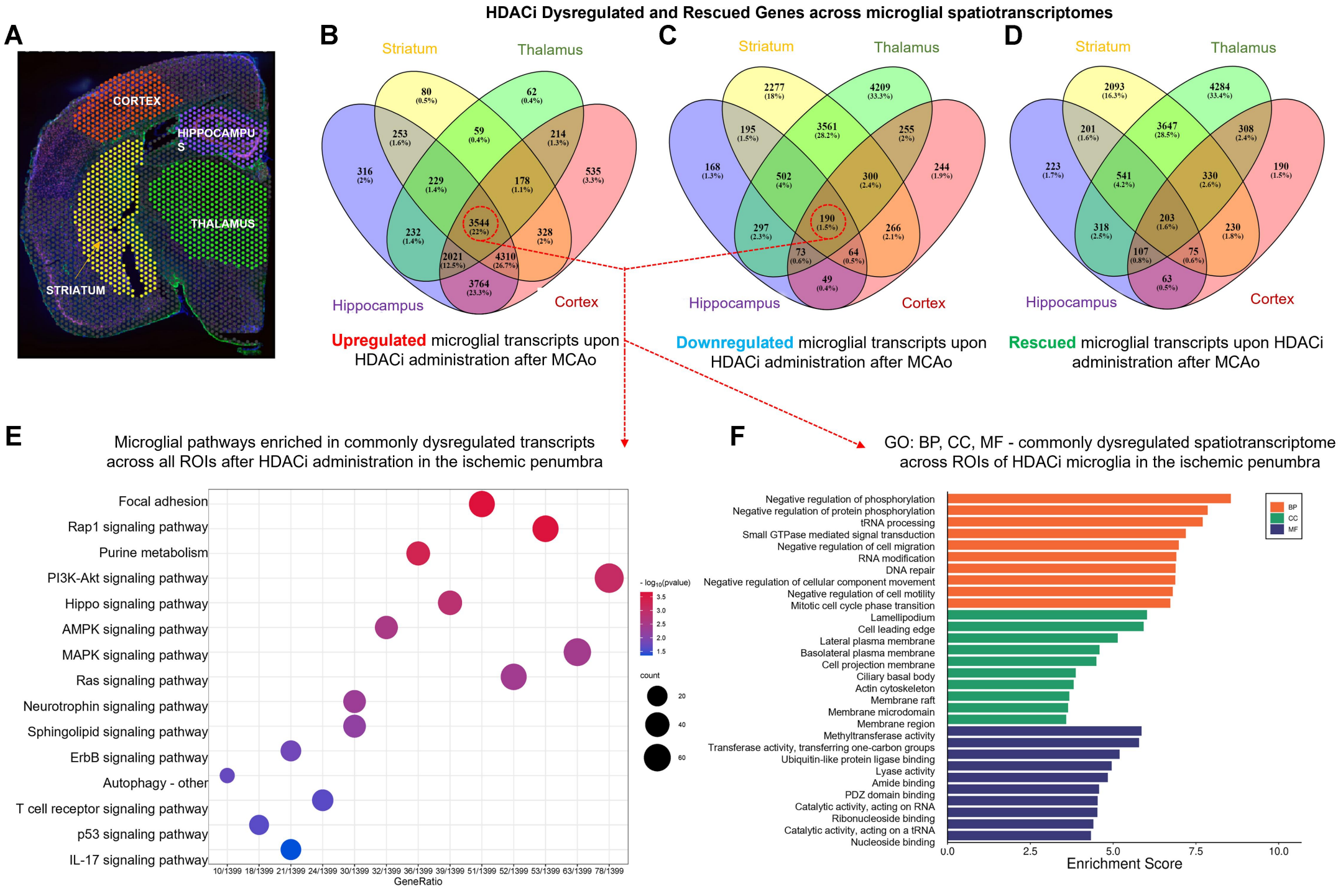
HDACi Dysregulated and Rescued Genes across microglial spatiotranscriptomes
A
CORTEX
HIPPOCAMPUS
THALAMUS
STRIATUM
B
Striatum
Thalamus
Hippocampus
Cortex
80 (0.5%)
62 (0.4%)
253 (1.6%)
59 (0.4%)
214 (1.3%)
316 (2%)
229 (1.4%)
178 (1.1%)
535 (3.3%)
232 (1.4%)
3544 (22%)
328 (2%)
2021 (12.5%)
4310 (26.7%)
3764 (23.3%)
Upregulated microglial transcripts upon HDACi administration after MCAo
C
Striatum
Thalamus
Hippocampus
Cortex
2277 (18%)
4209 (33.3%)
195 (1.5%)
3561 (28.2%)
255 (2%)
168 (1.3%)
502 (4%)
300 (2.4%)
244 (1.9%)
297 (2.3%)
190 (1.5%)
266 (2.1%)
73 (0.6%)
64 (0.5%)
49 (0.4%)
Downregulated microglial transcripts upon HDACi administration after MCAo
D
Striatum
Thalamus
Hippocampus
Cortex
2093 (16.3%)
4284 (33.4%)
201 (1.6%)
3647 (28.5%)
308 (2.4%)
223 (1.7%)
541 (4.2%)
330 (2.6%)
190 (1.5%)
318 (2.5%)
203 (1.6%)
230 (1.8%)
107 (0.8%)
75 (0.6%)
63 (0.5%)
Rescued microglial transcripts upon HDACi administration after MCAo
E
Microglial pathways enriched in commonly dysregulated transcripts across all ROIs after HDACi administration in the ischemic penumbra
Focal adhesion
Rap1 signaling pathway
Purine metabolism
PI3K-Akt signaling pathway
Hippo signaling pathway
AMPK signaling pathway
MAPK signaling pathway
Ras signaling pathway
Neurotrophin signaling pathway
Sphingolipid signaling pathway
ErbB signaling pathway
Autophagy - other
T cell receptor signaling pathway
p53 signaling pathway
IL-17 signaling pathway
10/1399 18/1399 21/1399 24/1399 30/1399 32/1399 36/1399 39/1399 51/1399 52/1399 53/1399 63/1399 78/1399
GeneRatio
- log10(pvalue)
3.5
3.0
2.5
2.0
1.5
count
20
40
60
F
GO: BP, CC, MF - commonly dysregulated spatiotranscriptome across ROIs of HDACi microglia in the ischemic penumbra
Negative regulation of phosphorylation
Negative regulation of protein phosphorylation
tRNA processing
Small GTPase mediated signal transduction
Negative regulation of cell migration
RNA modification
DNA repair
Negative regulation of cellular component movement
Negative regulation of cell motility
Mitotic cell cycle phase transition
Lamellipodium
Cell leading edge
Lateral plasma membrane
Basolateral plasma membrane
Cell projection membrane
Ciliary basal body
Actin cytoskeleton
Membrane raft
Membrane microdomain
Membrane region
Methyltransferase activity
Transferase activity, transferring one-carbon groups
Ubiquitin-like protein ligase binding
Lyase activity
Amide binding
PDZ domain binding
Catalytic activity, acting on RNA
Ribonucleoside binding
Catalytic activity, acting on a tRNA
Nucleoside binding
0.0
2.5
5.0
7.5
10.0
Enrichment Score
BP
CC
MF

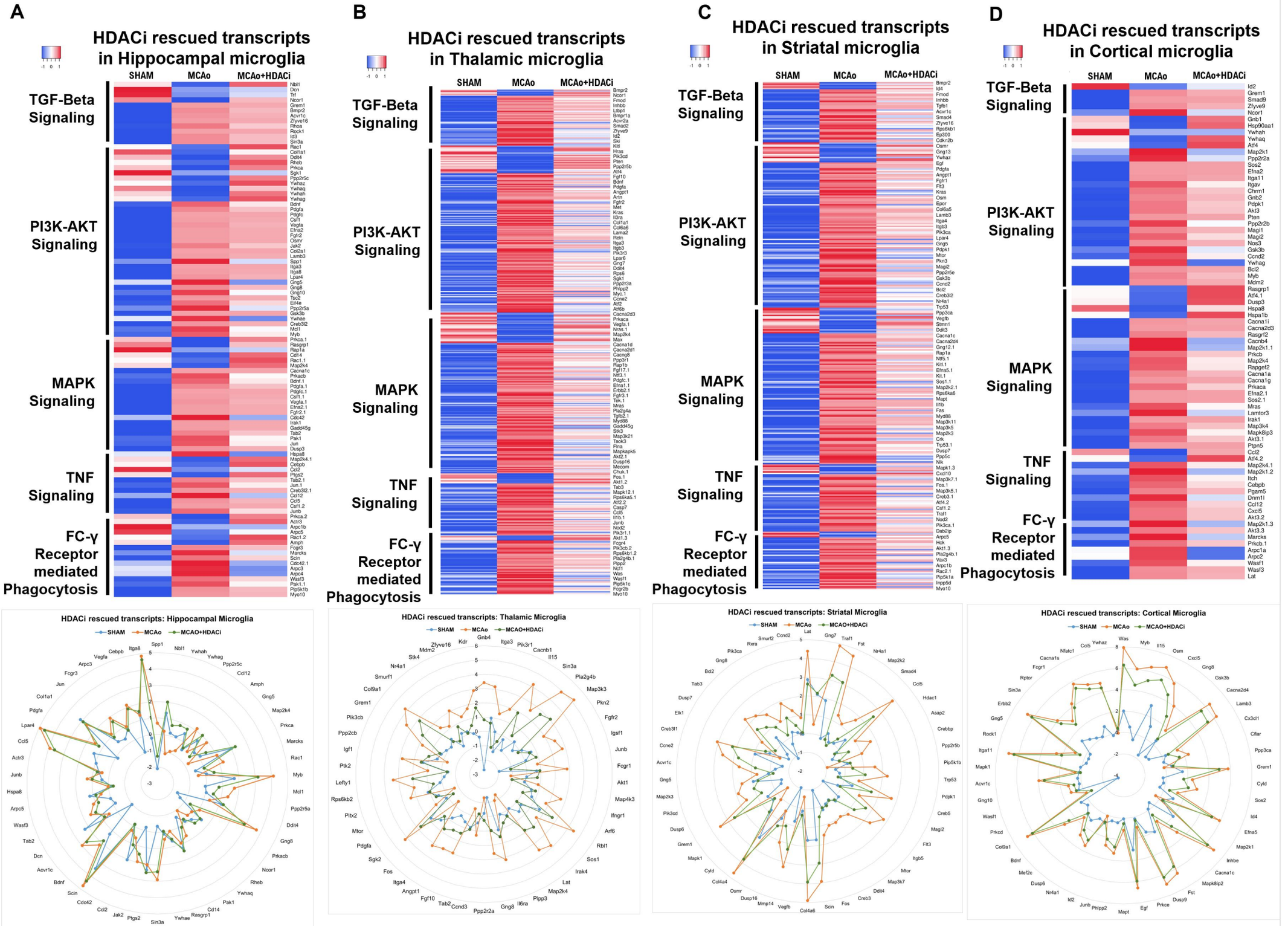
A
HDACi rescued transcripts in Hippocampal microglia
SHAM
MCAo
MCAo+HDACi
TGF-Beta Signaling
PI3K-AKT Signaling
MAPK Signaling
TNF Signaling
FC-γ Receptor mediated Phagocytosis
B
HDACi rescued transcripts in Thalamic microglia
C
HDACi rescued transcripts in Striatal microglia
D
HDACi rescued transcripts in Cortical microglia
HDACi rescued transcripts: Hippocampal Microglia
HDACi rescued transcripts: Thalamic Microglia
HDACi rescued transcripts: Striatal Microglia
HDACi rescued transcripts: Cortical Microglia

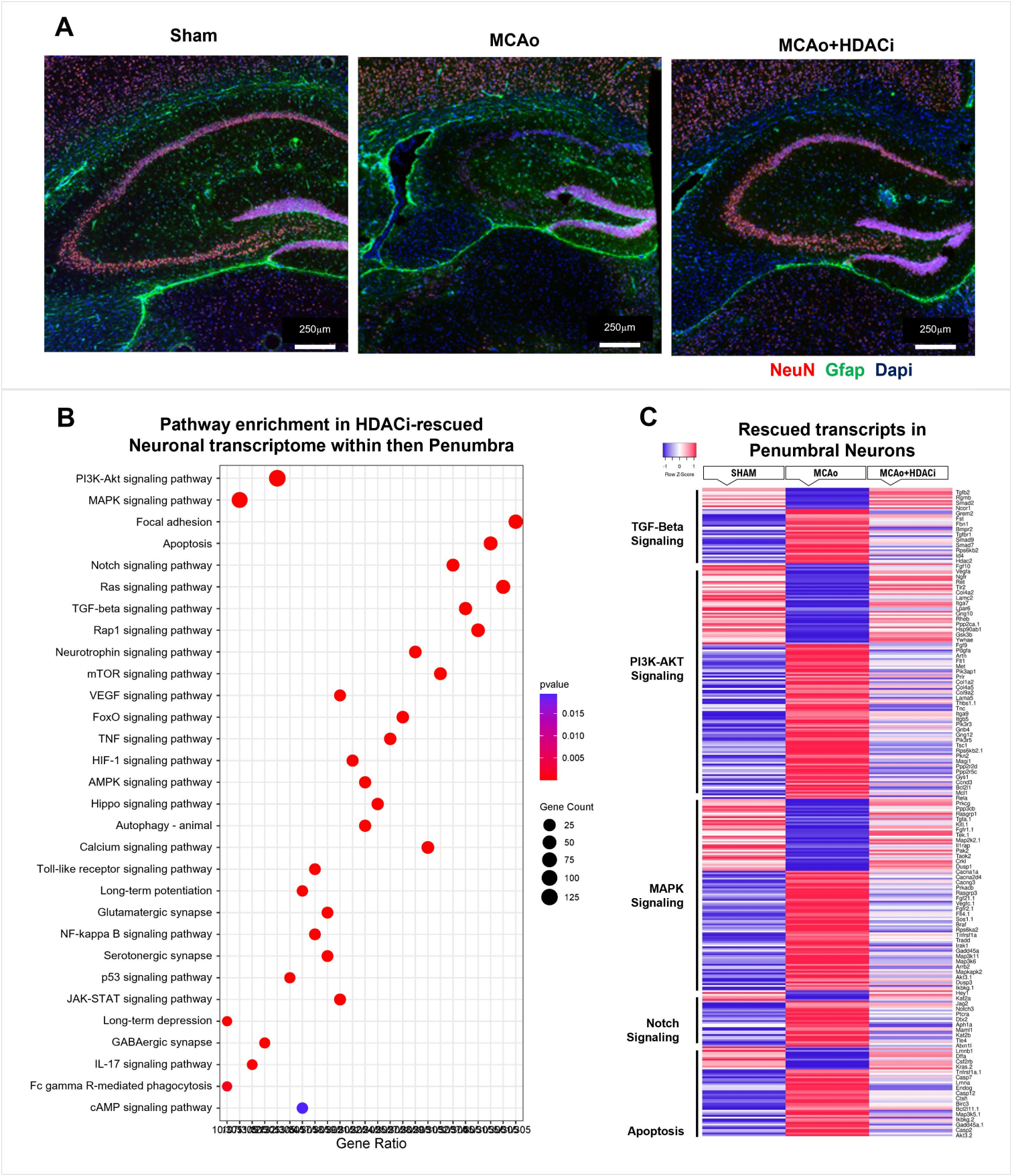
A
Sham
MCAo
MCAo+HDACi
250μm
250μm
250μm
NeuN Gfap Dapi
B
Pathway enrichment in HDACi-rescued
Neuronal transcriptome within then Penumbra
PI3K-Akt signaling pathway
MAPK signaling pathway
Focal adhesion
Apoptosis
Notch signaling pathway
Ras signaling pathway
TGF-beta signaling pathway
Rap1 signaling pathway
Neurotrophin signaling pathway
mTOR signaling pathway
VEGF signaling pathway
FoxO signaling pathway
TNF signaling pathway
HIF-1 signaling pathway
AMPK signaling pathway
Hippo signaling pathway
Autophagy - animal
Calcium signaling pathway
Toll-like receptor signaling pathway
Long-term potentiation
Glutamatergic synapse
NF-kappa B signaling pathway
Serotonergic synapse
p53 signaling pathway
JAK-STAT signaling pathway
Long-term depression
GABAergic synapse
IL-17 signaling pathway
Fc gamma R-mediated phagocytosis
cAMP signaling pathway
Gene Ratio
pvalue
0.015
0.010
0.005
Gene Count
25
50
75
100
125
C
Rescued transcripts in
Penumbral Neurons
Row Z-Score
SHAM
MCAo
MCAo+HDACi
TGF-Beta Signaling
PI3K-AKT Signaling
MAPK Signaling
Notch Signaling
Apoptosis

Figure 1 Supplementary Figure 1

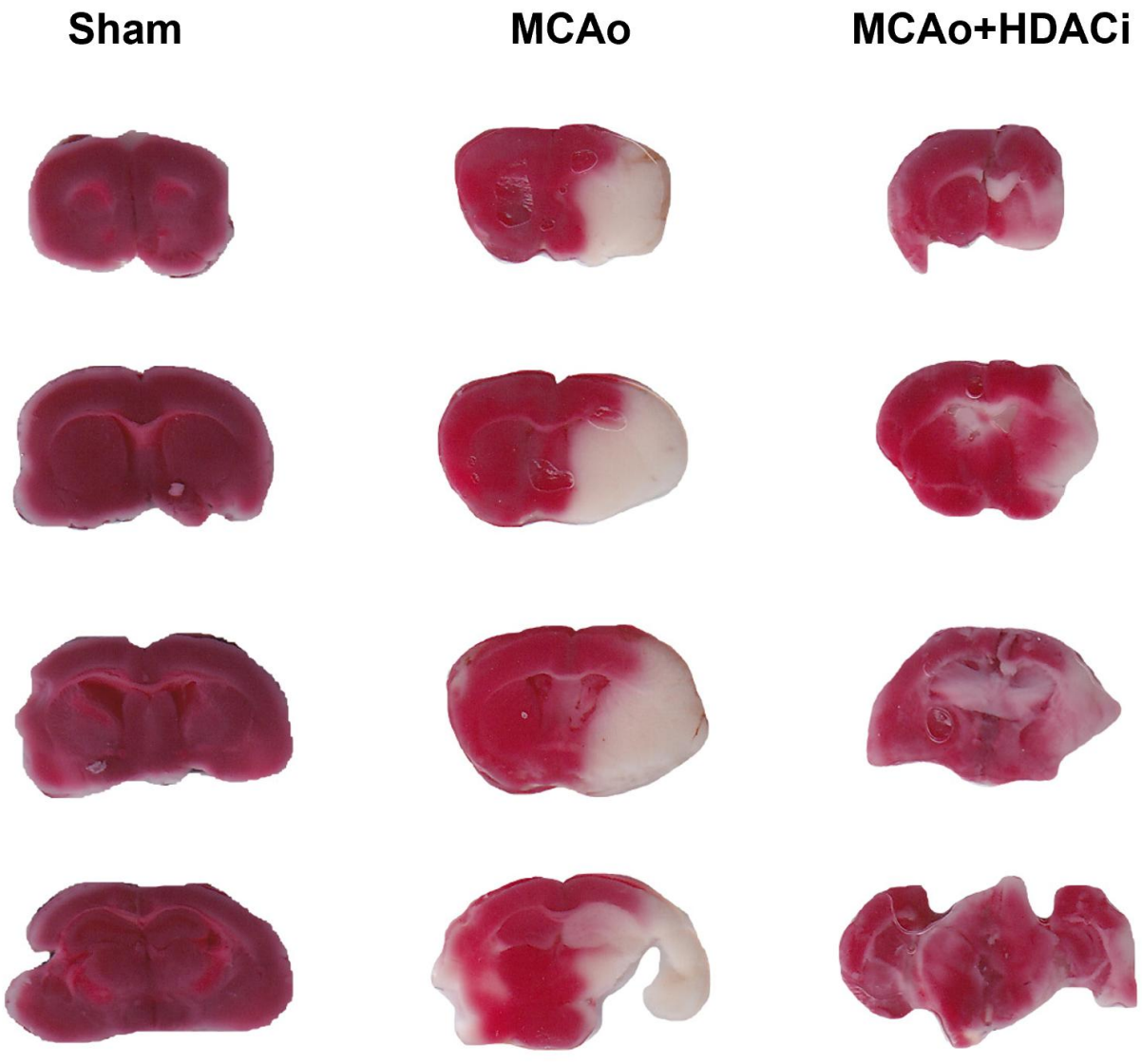

TTC (2,3,5-Triphenyltetrazolium Chloride)

Figure 3 Supplementary Figure 1

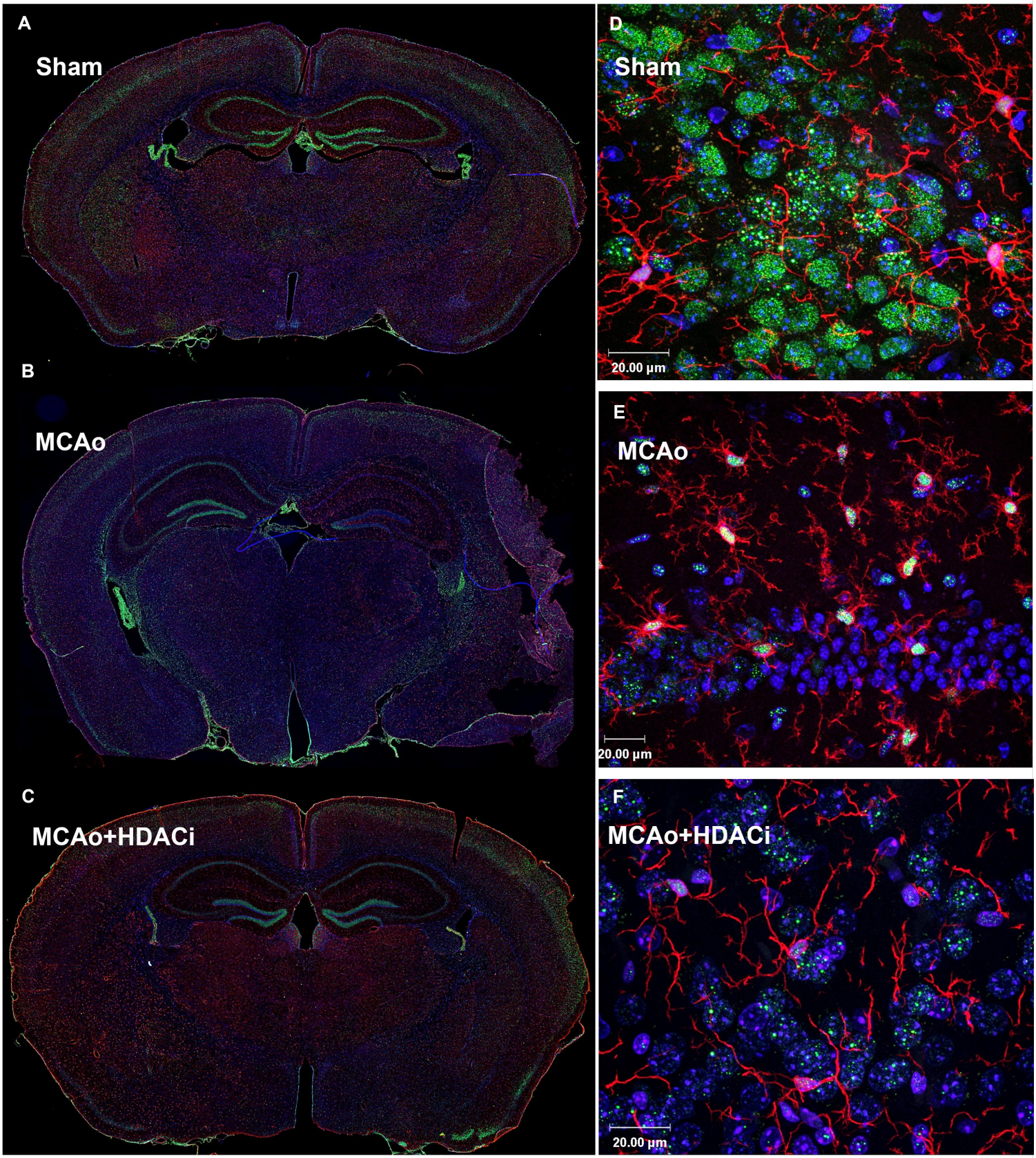

Figure 4 Supplementary Figure 1

A

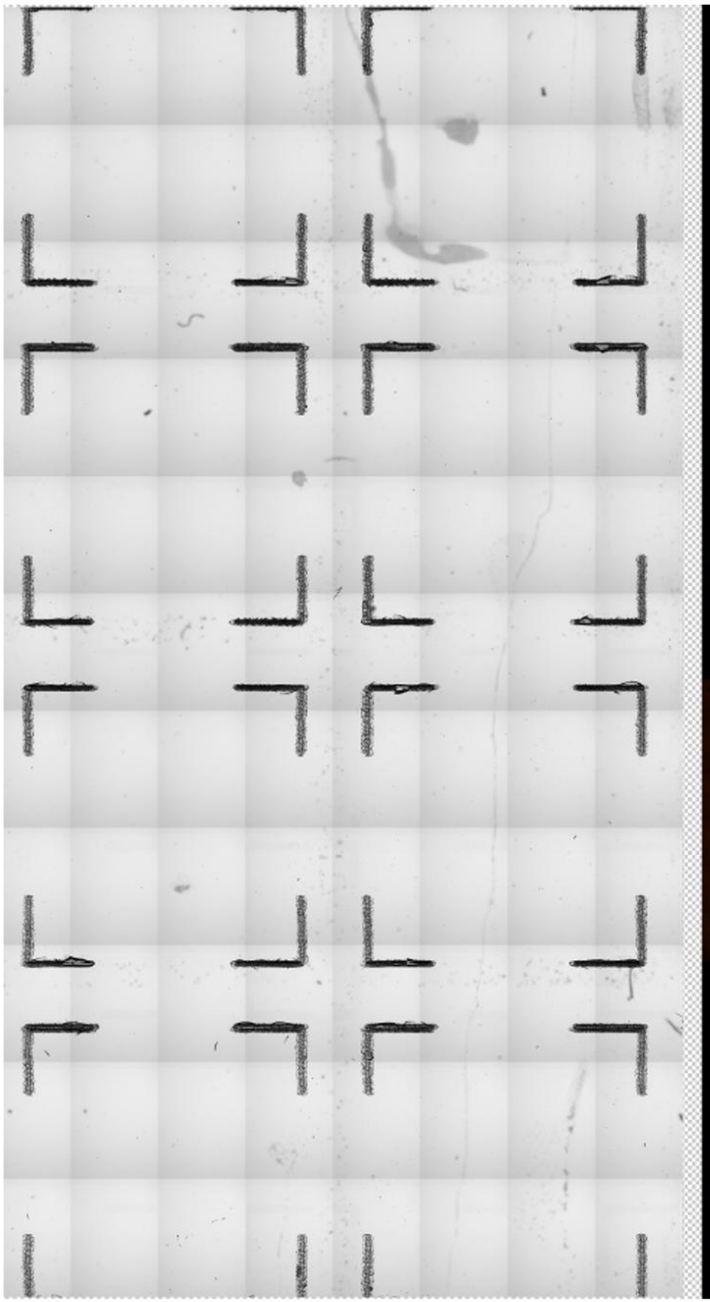

B

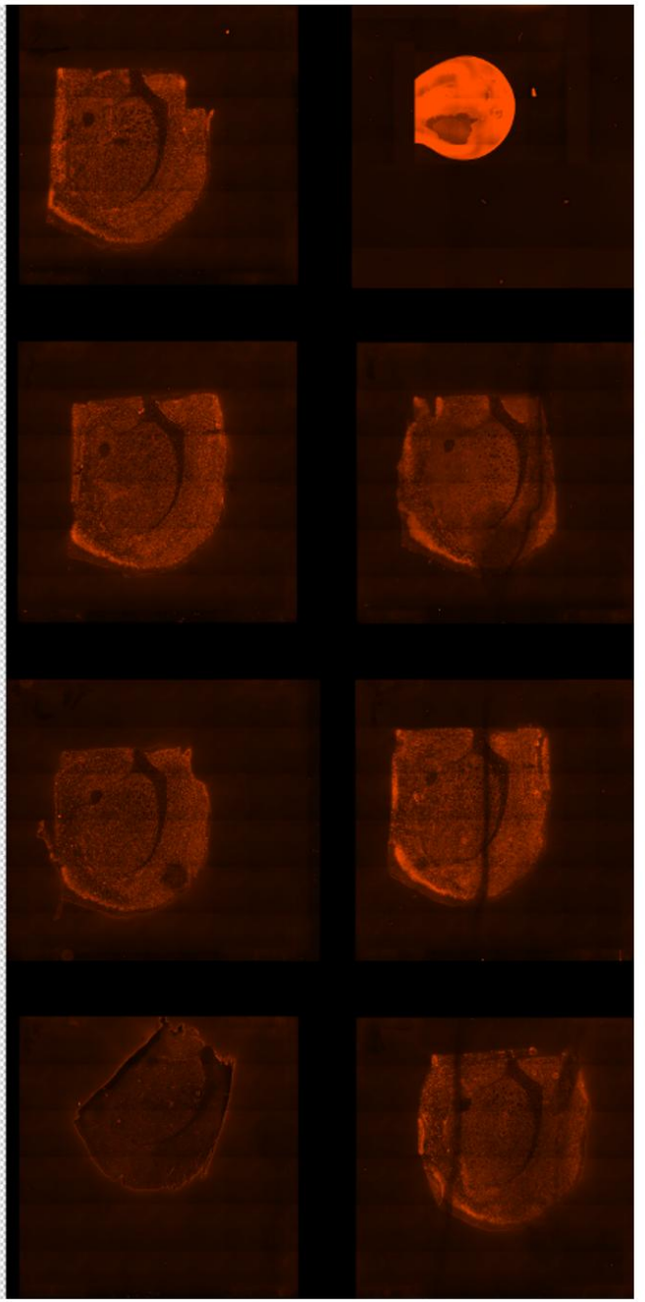

C

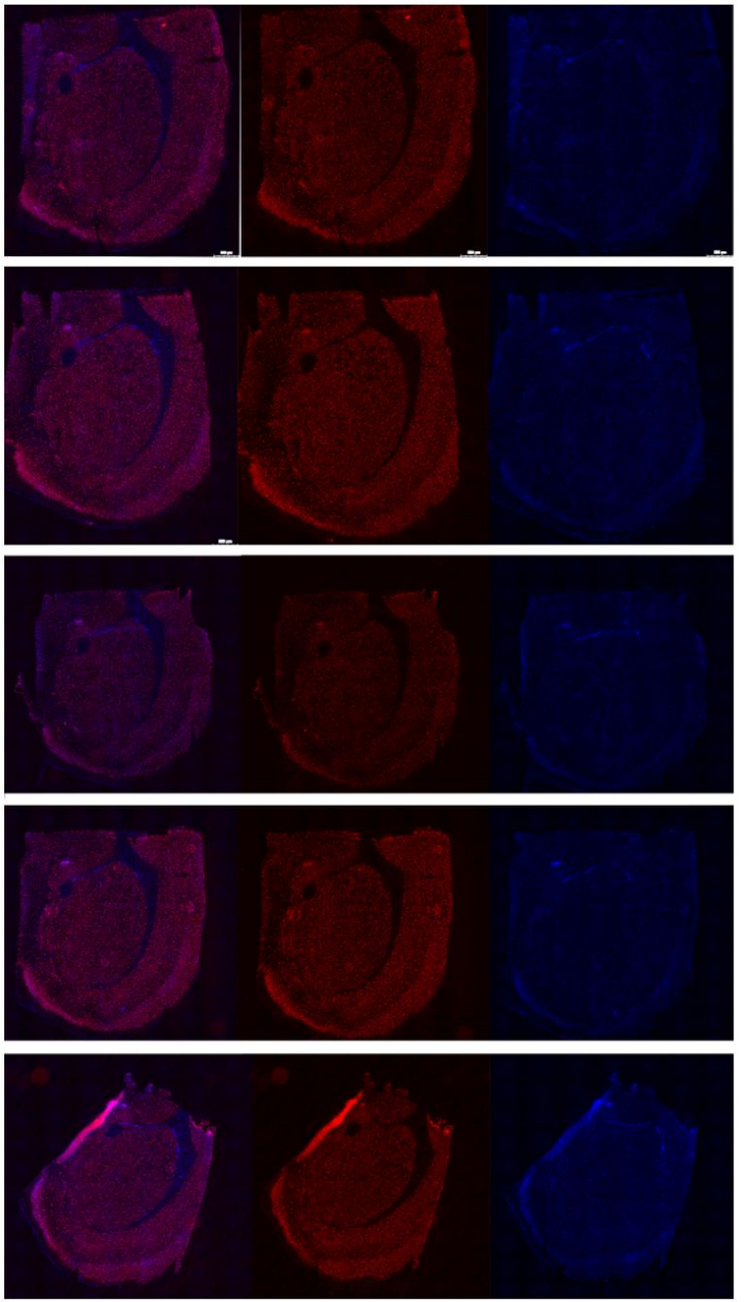

Figure 4 Supplementary Figure 2

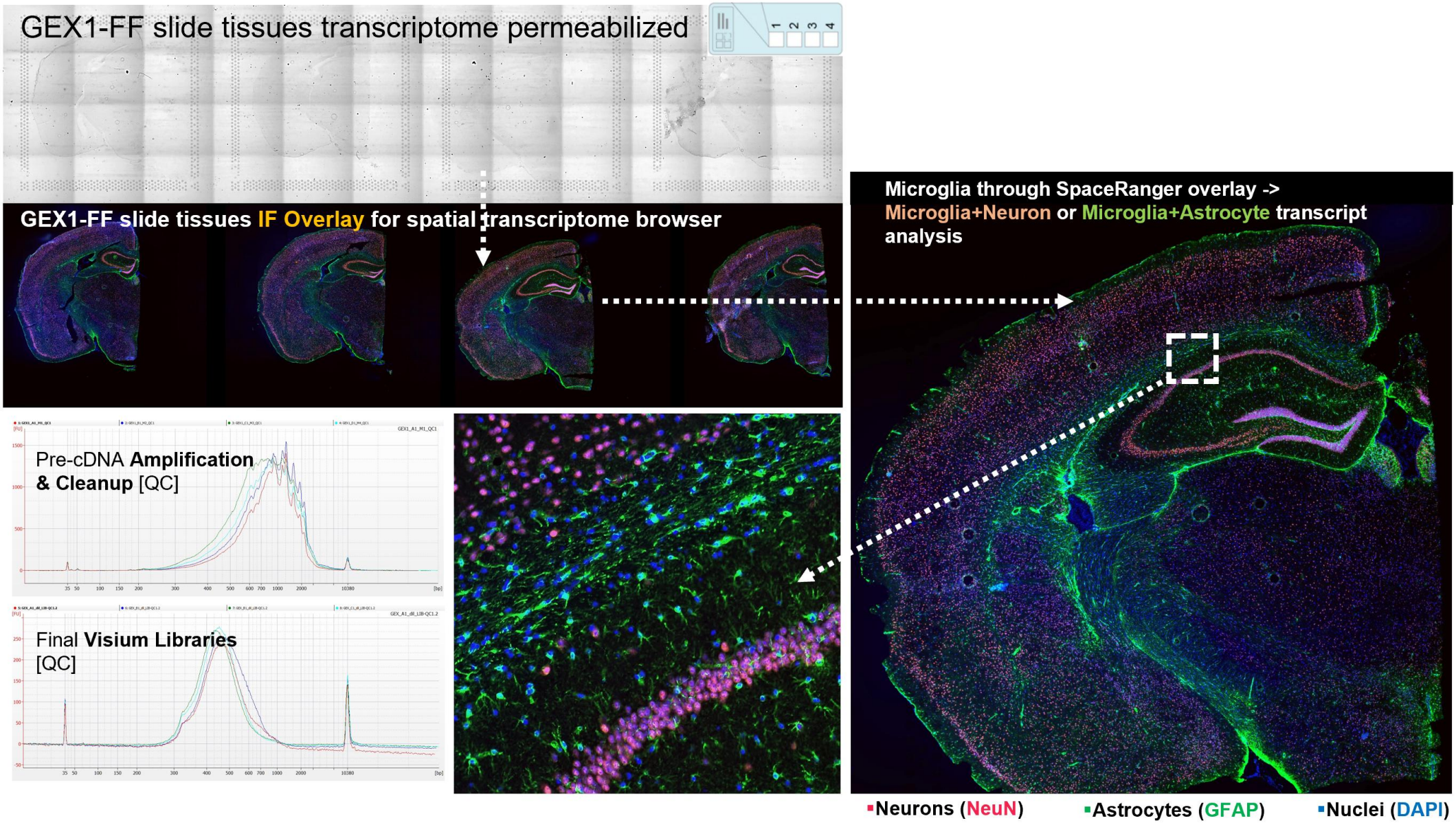

Figure 5 Supplementary Figure 1

IL-17 Signaling | Autophagy | Hippo Signaling | Neurotrophin Signaling pathways

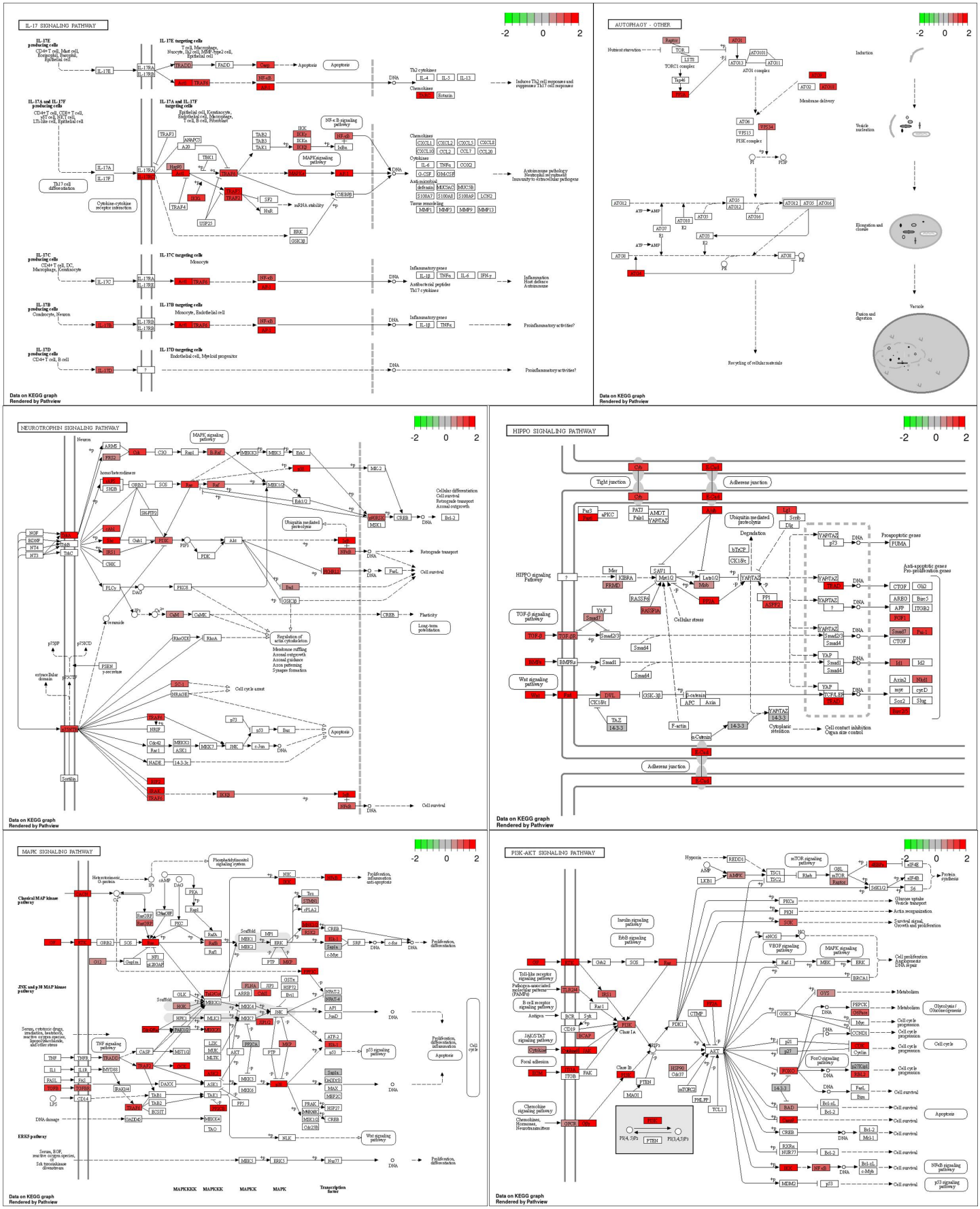

Figure 6 Supplementary Figure 1A

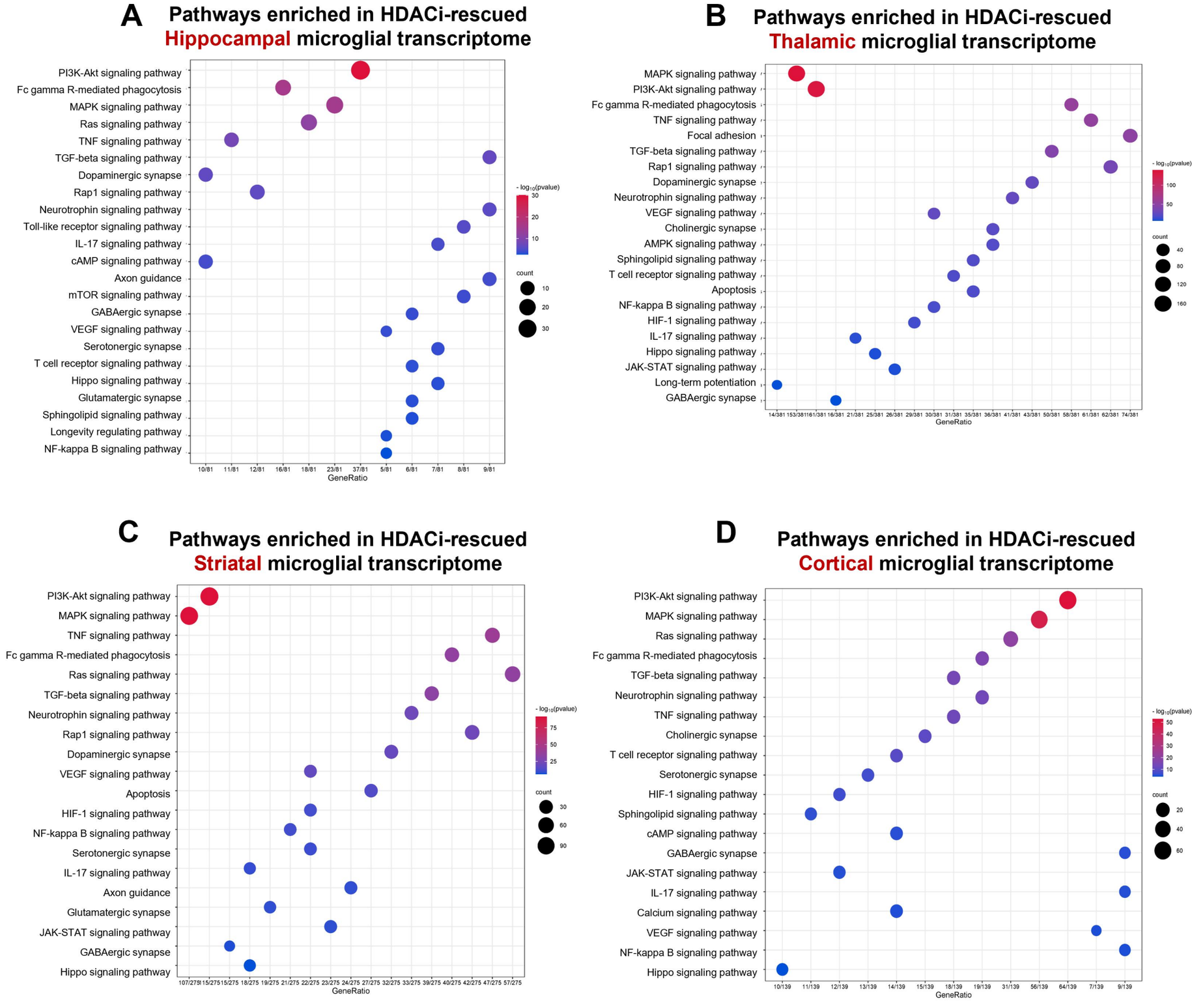

Figure 6 Supplementary Figure 1B

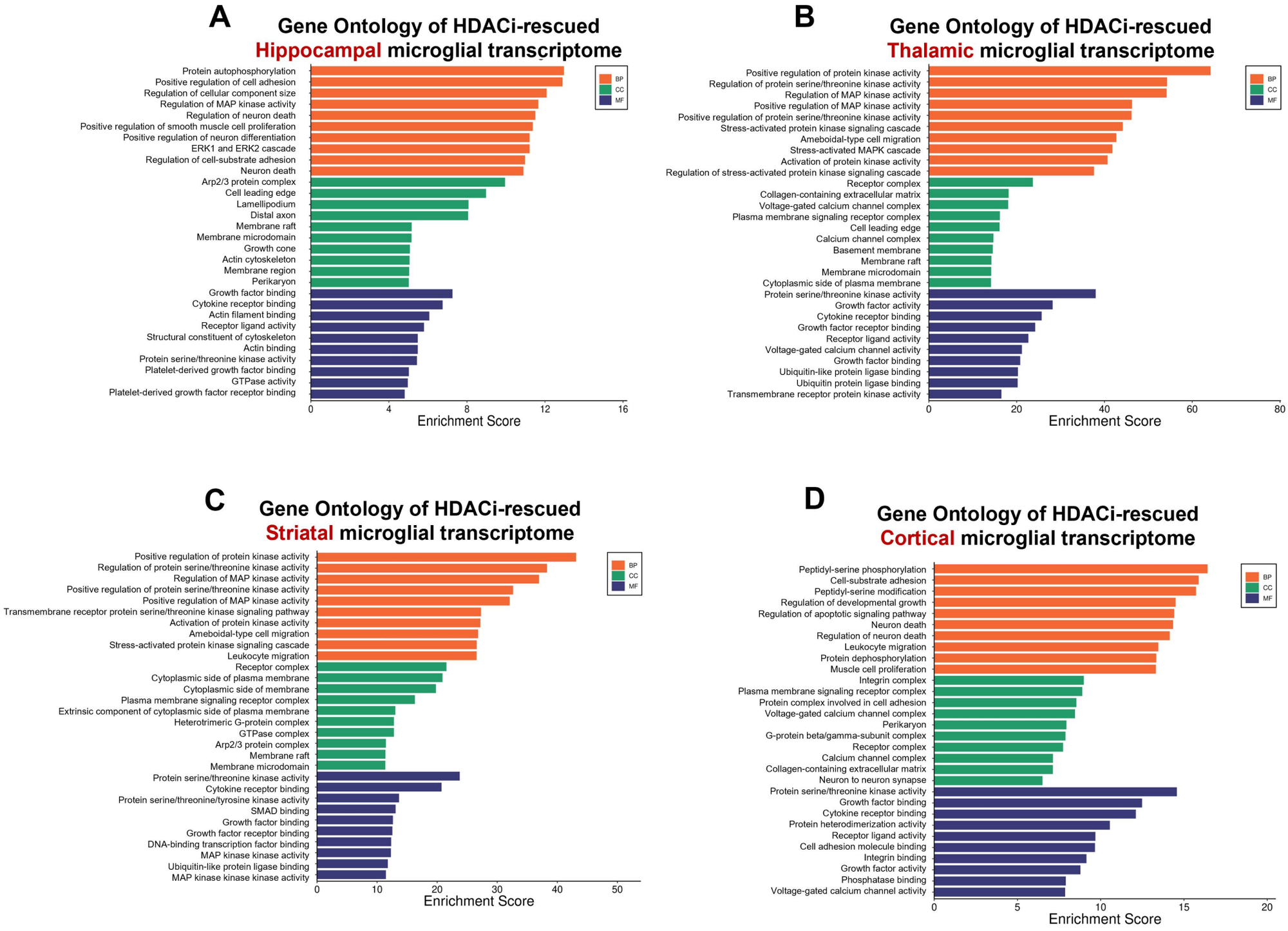

Figure 6 Supplementary Figure 2

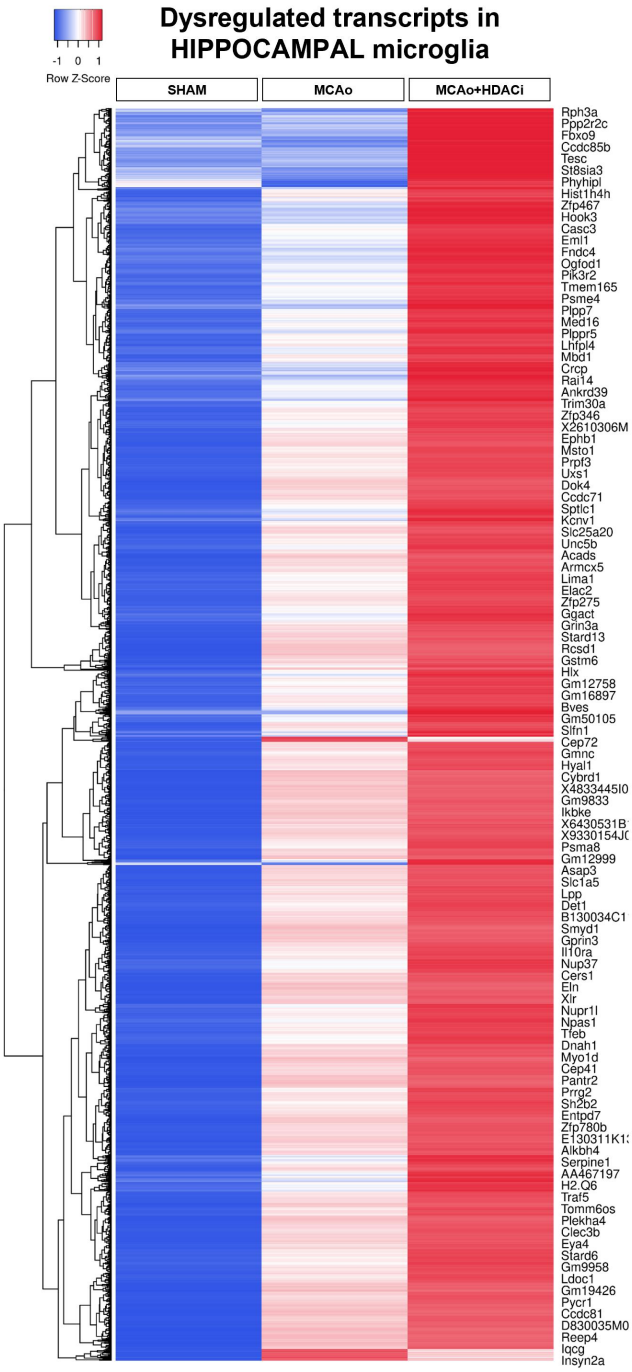

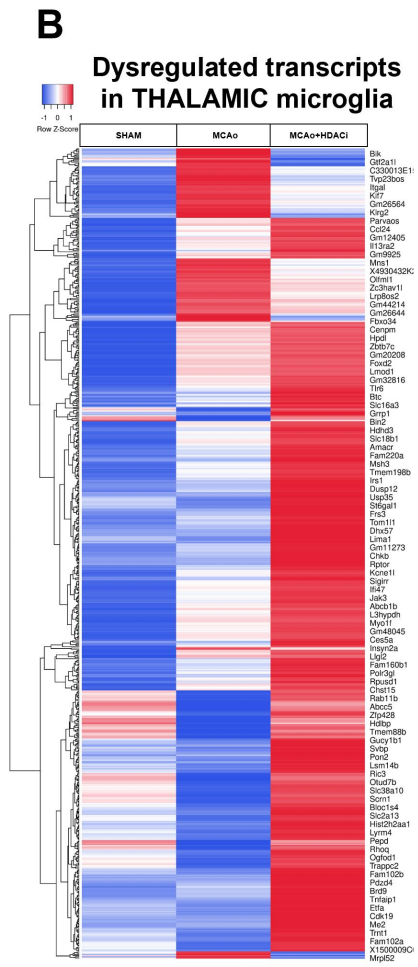

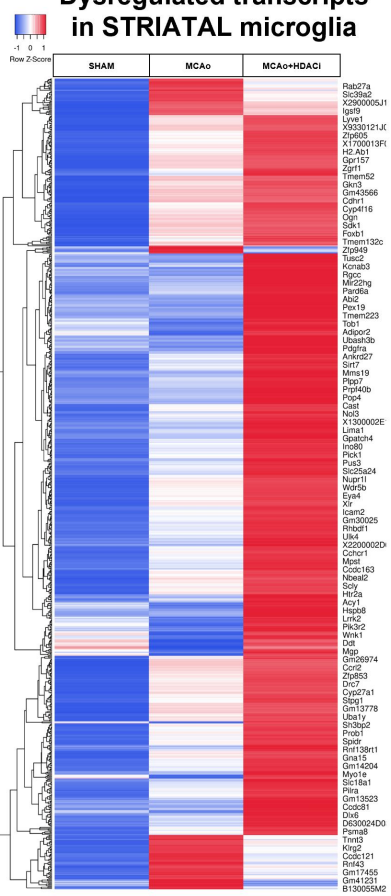

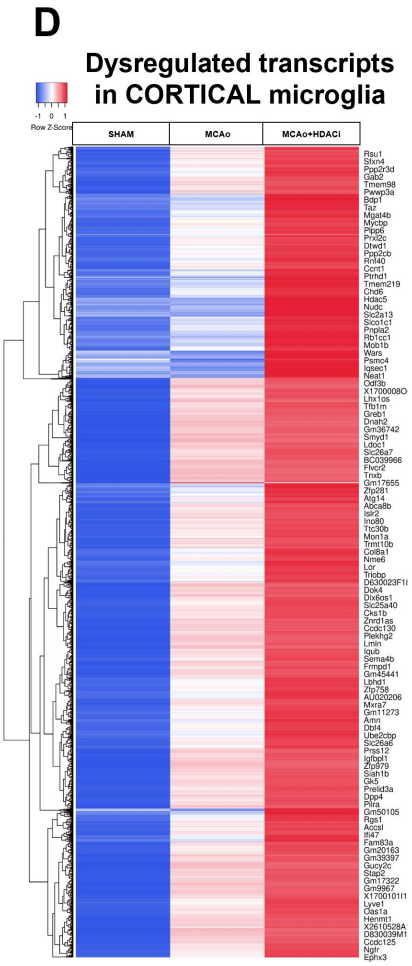

E

Key dysregulated transcripts

TGF-beta Pathway:	TNF-alpha Pathway:	PI3K-AKT Pathway:	FC-Receptor Mediated Phagocytosis:	MAPK Signaling Pathway:
TGFBR1	TNF	PIK3CA	FCGR1	MAPK1 (ERK2)
TGFBR2	NFkB1 (p50)	PIK3CB	FCGR3	MAPK3 (ERK1)
SMAD2	RELA (p65)	AKT1	FCGR4	DUSP1
SMAD3		AKT2	SYK	DUSP4
SMAD4		AKT3	PIP5K1C	DUSP6
TGFB1		PTEN		
TGFB2				
TGFB3				
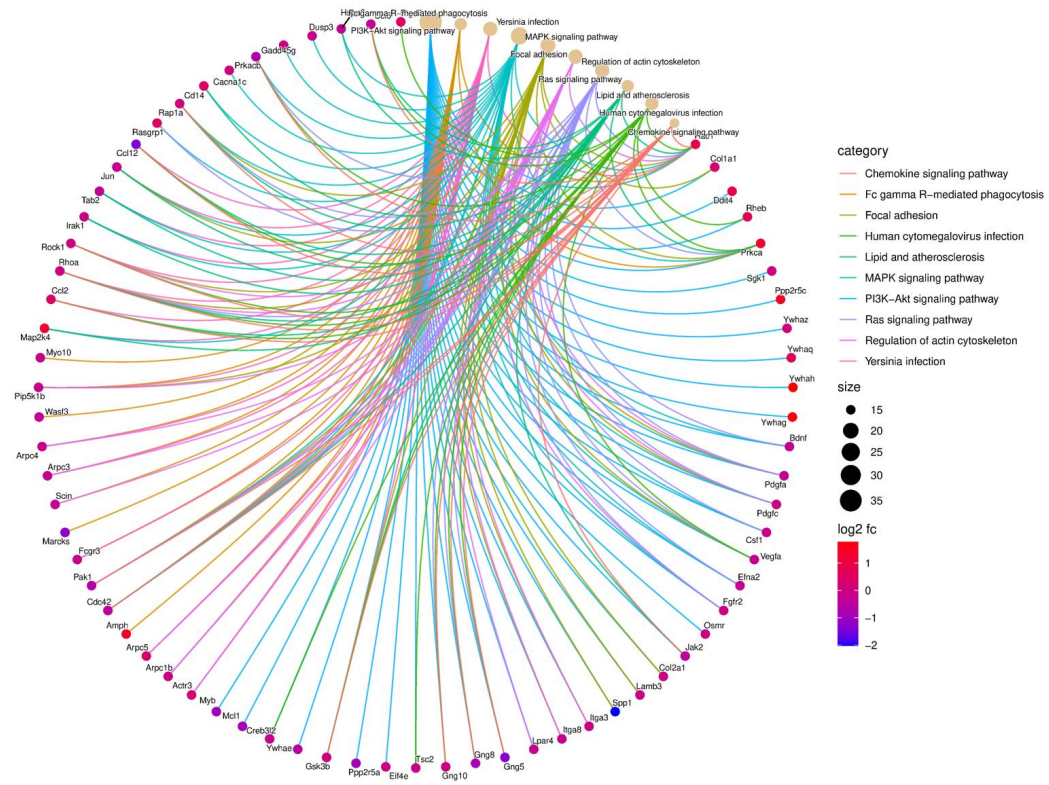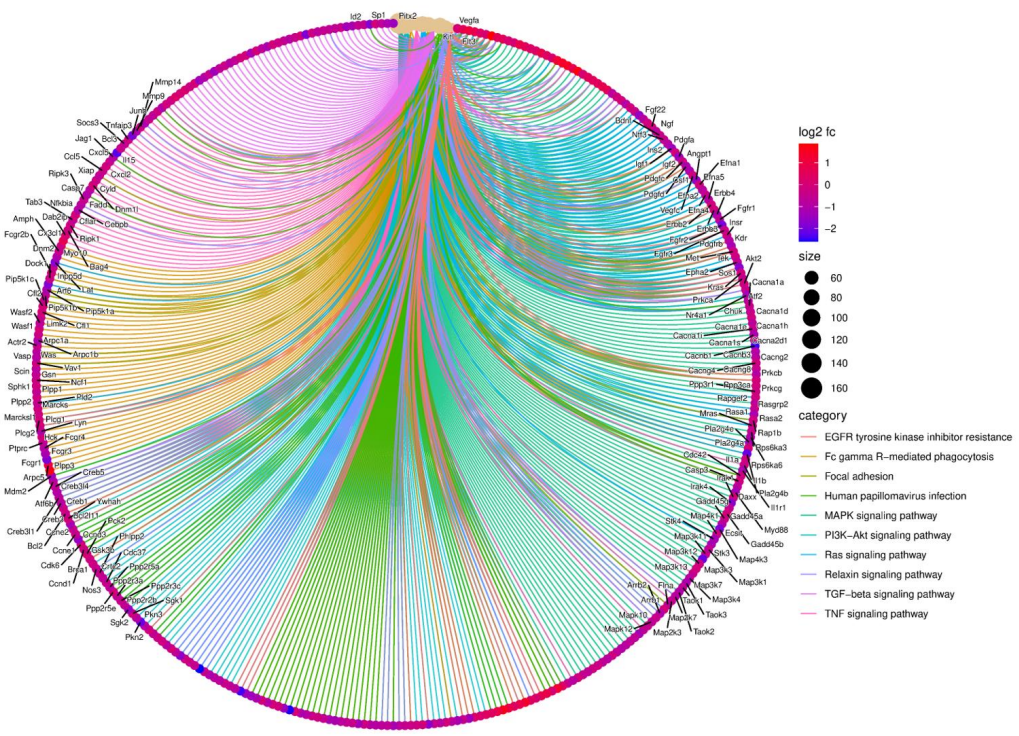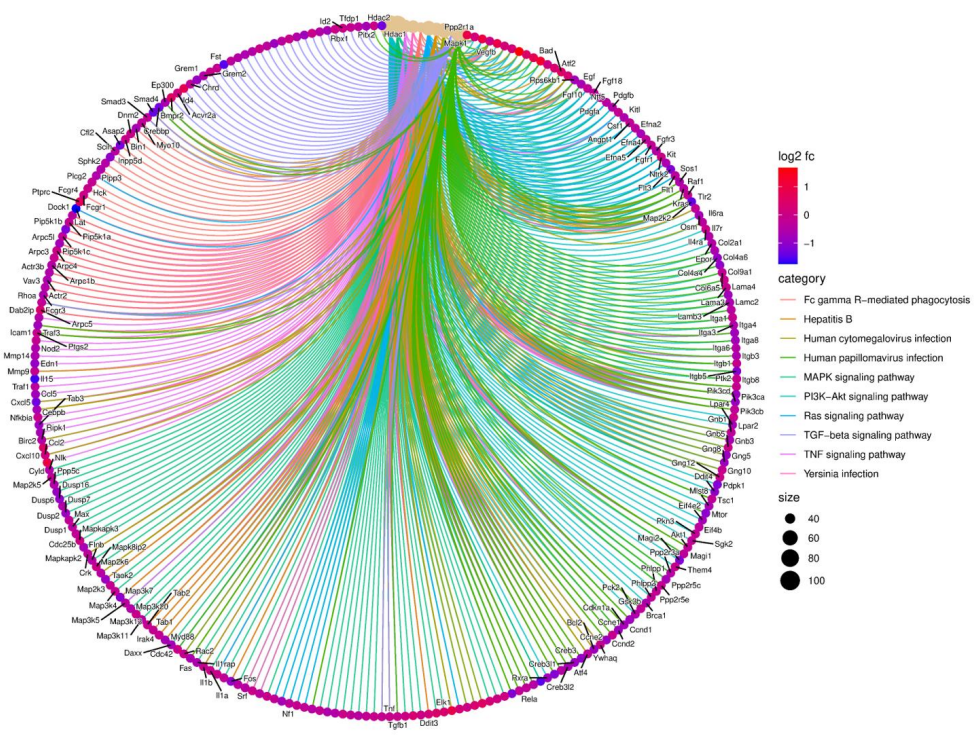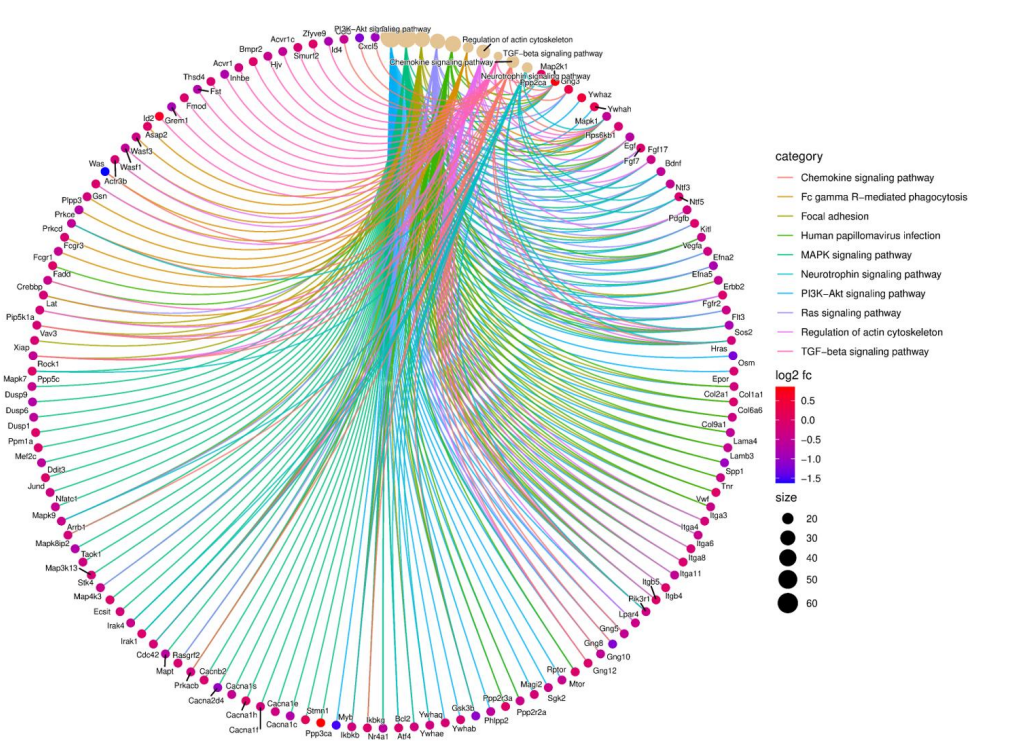
Figure 6 Supplementary Figure 3